
Diffusion-Inspired Reconfiguration of Transformers for Uncertainty Calibration

Manh Cuong Dao*
National University of Singapore

Quang Hung Pham*
Hanoi University of Science and Technology

Phi Le Nguyen
Hanoi University of Science and Technology

Thao Nguyen Truong
National Institute of Advanced Industrial Science and Technology

Bryan Kian Hsiang Low
National University of Singapore

Trong Nghia Hoang[†]
Washington State University

Abstract

Uncertainty calibration in pre-trained transformers is critical for their reliable deployment in risk-sensitive applications. Yet, most existing pre-trained transformers do not have a principled mechanism for uncertainty propagation through their feature transformation stack. In this work, we propose a diffusion-inspired reconfiguration of transformers in which each feature transformation block is modeled as a probabilistic mapping. Composing these probabilistic mappings reveals a probability path that mimics the structure of a diffusion process, transporting data mass from the input distribution to the pre-trained feature distribution. This probability path can then be recompiled on a diffusion process with a unified transition model to enable principled propagation of representation uncertainty throughout the pre-trained model’s architecture while maintaining its original predictive performance. Empirical results across a variety of vision and language benchmarks demonstrate that our method achieves superior calibration and predictive accuracy compared to existing uncertainty-aware transformers.

1 Introduction

The transformer architecture [66] has become a universal backbone in most large-scale pre-trained or foundation models spanning numerous domains. These include language [17, 50, 8, 2, 60], vision [18, 59, 37], speech [4, 29, 49], and even more complex domains with multi-modal data (e.g., text-image) [48, 35, 19, 58].

Challenge. Despite their prevalence, existing transformer-based models lack a principled mechanism to assess prediction uncertainty. This often leads to incorrect predictions being assigned high confidence [22, 43] which raises safety concerns in high-stake applications [41, 74]. Uncertainty calibration (UC), or confidence calibration, addresses this issue by ensuring that a model’s predicted confidence faithfully reflects its empirical accuracy, thereby making confidence scores reliable for downstream decision-making. For example, effective UC techniques can help determine when to defer to human experts in scenarios where the model exhibits high representation and/or prediction

*Equal contribution.

[†]Corresponding author.

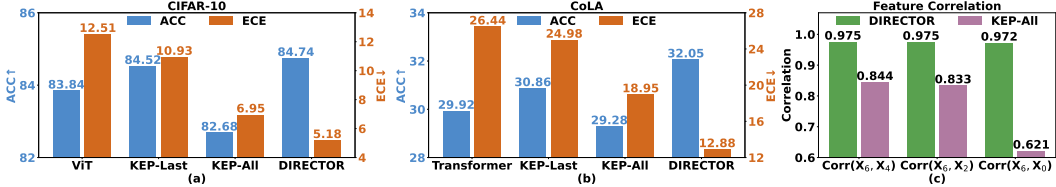


Figure 1: Comparison of accuracy (ACC \uparrow) and uncertainty calibration (ECE \downarrow) across pretrained models (ViT, Transformer), GP-reparameterized method KEP [15] applied to either the last attention block (KEP-last) or all attention blocks (KEP-All), and our method (DIRECTOR) on (a) CIFAR-10 and (b) CoLA dataset. Panel (c) compares the correlation between features at the first layer (X_6) and those at deeper layers (X_4 , X_2 , and X_0 at the last layer) for DIRECTOR and KEP-All on CIFAR-10 dataset.

uncertainty, particularly in risk-sensitive applications [63, 54, 55]. While UC has been extensively studied in conventional low-complexity deep neural networks, existing techniques mainly focus on imposing probabilistic priors on network weights and approximating their posteriors via either variational inference or posterior sampling. This quickly becomes both inaccurate and prohibitively expensive when the model complexity increases.

Emerging Paradigm. To sidestep the challenge of computing posteriors over models with exceedingly large complexities, there are emerging approaches that aim to reparameterize the attention outputs as (sparse) Gaussian process predictions [36, 12, 9, 15] and recast the pre-trained transformer as a probabilistic chain mapping from the data distribution to a feature distribution. This enables principled, uncertainty-aware sampling of feature representations by simulating the chain rather than inferring them via computing the prohibitively expensive model posterior, thereby motivating a more scalable paradigm for UC in large models.

Research Gap. Intuitively, separate reparameterization fails to account for the correlations among feature transformations at different attention blocks that were established during pre-training. This results in an unfavorable exchange between uncertainty calibration and performance. Previous approaches that adopt separate re-parameterization often improve uncertainty calibration at the cost of significantly reduced performance (see Fig. 1a, 1b), which does not align with the expectation that improved uncertainty calibration should, in general, lead to improved performance. From the above intuition, this is not surprising since accurate uncertainty propagation means being able to properly account for the high correlation across feature transformation steps. This is however not upheld in previous approaches according to our investigation. For instance, our results in Fig. 1c show that the correlation between the feature at the first KEP-SVGP’s layer and intermediate representations rapidly decreases as it is propagated further towards the solution head. In contrast, our proposed method DIRECTOR manages to correctly preserve this high correlation. As a result, Fig. 1 shows that DIRECTOR indeed improves uncertainty calibration while also improving performance as expected.

Solution Vision. To address this gap, we propose distilling the sequence of reparameterized attention blocks into a unified diffusion model. Rather than treating each block as an independent reparameterization, we model the entire sequence as a continuous stochastic process over the feature embedding space. In this view, the observed transformations of a pre-trained model are interpreted as samples from a diffusion process governed by a single spatiotemporal transition kernel that maps the data distribution to the final representation. This unified view allows us to capture cross-block correlations established during pre-training while providing a principled mechanism for propagating uncertainty.

Technical Contributions. To substantiate this vision, we develop a diffusion-based framework for unified uncertainty propagation across transformer blocks with the following technical contributions:

1. We reinterpret the step-wise feature transformations of a pre-trained transformer as transition samples from a probabilistic path that maps the data distribution to the feature distribution. This perspective generalizes the transformer into a diffusion model parameterized by a unified transition kernel, which can be learned from these observed transitions. Such reconfiguration supports local uncertainty calibration at individual attention blocks while ensuring an accurate flow of uncertainty propagation across the entire network (see Section 2.1).
2. We design a training algorithm that distills the observed sequence of feature transformations into a unified spatiotemporal transition kernel of a diffusion process. The learned kernel captures

the inherent correlations among feature transformations across attention blocks established during pre-training, providing a tractable and principled procedure for uncertainty calibration in large pre-trained models. This allows us to establish a generative paradigm for UC, where uncertainty-aware representation samples are drawn directly from the learned diffusion process rather than inferred via intractable model posteriors (see Section 2.2).

3. We conduct extensive experiments on vision and language benchmarks to evaluate calibration quality, robustness, and out-of-distribution (OOD) detection. The results show that our approach consistently improves uncertainty calibration while preserving predictive performance over existing state-of-the-art pre-trained transformer models. Remarkably, it achieves these gains with fewer parameters than the original model, leading to improved memory efficiency. These results demonstrate the feasibility of post-hoc embedding probabilistic reasoning into the internal structure of large pre-trained models for uncertainty calibration without sacrificing performance. This opens a new direction for enhancing their reliability in safety-critical settings (see Section 3).

2 Diffusion-Inspired Reconfiguration of Transformers

Recent efforts to incorporate uncertainty into transformer-based models have uncovered a connection between multi-head self-attention (MHSA) and Gaussian processes (GPs) which shows that the deterministic output of a MHSA block corresponds to the posterior mean of a GP conditioned on its input [12, 9, 15] (see Appendix A.2). Although this insight offers a principled approach for uncertainty calibration at individual attention blocks, propagating it across MHSA blocks remain challenging. The difficulty arises because GP-reparameterized MHSA is interleaved with point-estimated components such as feed-forward networks (MLP) and layer normalization (LN). This disrupts the flow of uncertainty propagation since the interleaved sequence does not align with a well-defined stochastic path with a proper probabilistic transition model, particularly along the point-estimated segments of the pre-trained model.

To enable principled uncertainty propagation in pre-trained transformers, we instead propose a structural reconfiguration that reorganizes the model into a well-defined probabilistic path. In particular, we repartition the architecture such that each transformation block ends with an MHSA block (see Fig. 2), whose output can be interpreted as a Gaussian distribution over intermediate features. This restructuring instead views the aforementioned point-estimated network segments as additional parameterization of a GP-reparameterized MHSA rather than observations of a latent probabilistic transition (see Section 2.1). The resulting sequence of neuralized Gaussian transitions thus becomes well-aligned with the reverse-time stochastic process of a diffusion model.

These neuralized Gaussian transitions can then be viewed as discrete observations at different time steps of the diffusion’s reverse-time process. We can thus learn this process via distilling these observed transition across different timesteps into a unified spatiotemporal transition kernel. This can be achieved via adopting variational inference as inspired by score-based diffusion methods [57, 28]. This reveals a novel reconfiguration of pre-trained transformers into uncertainty-aware diffusion processes that interestingly enables UC via learning generative models translating between raw data and predictive features (see Section 2.2).

2.1 Reconfiguring Pre-Trained Transformer as Probability Path

Following prior work on uncertainty-aware transformers [12, 9, 15], the output of a kernelized attention head can be interpreted as the predictive mean at the input queries of a Gaussian process (GP) posterior conditioned on the key-value pairs. This means kernelizing attention transforms the original MHSA mechanism into a GP-based variant that naturally incorporates calibrated uncertainty. Each attention head thus admits a reparameterized Gaussian process (GP) structure which induces a neuralized Gaussian transition,

$$\mathbf{F}_t^{(h)} | \mathbf{U}_t \sim \mathbb{N} \left(\bar{m}_t^{(h)}(\mathbf{U}_t), \bar{\sigma}_t^{(h)}(\mathbf{U}_t) \right), \quad (1)$$

where \mathbf{U}_t is the input of the t -th MHSA block whereas $\bar{m}_t^{(h)}(\mathbf{U}_t), \bar{\sigma}_t^{(h)}(\mathbf{U}_t)$ are neuralized mean and covariance functions for its h -th attention head under the reparameterization design (Appendix A.2).

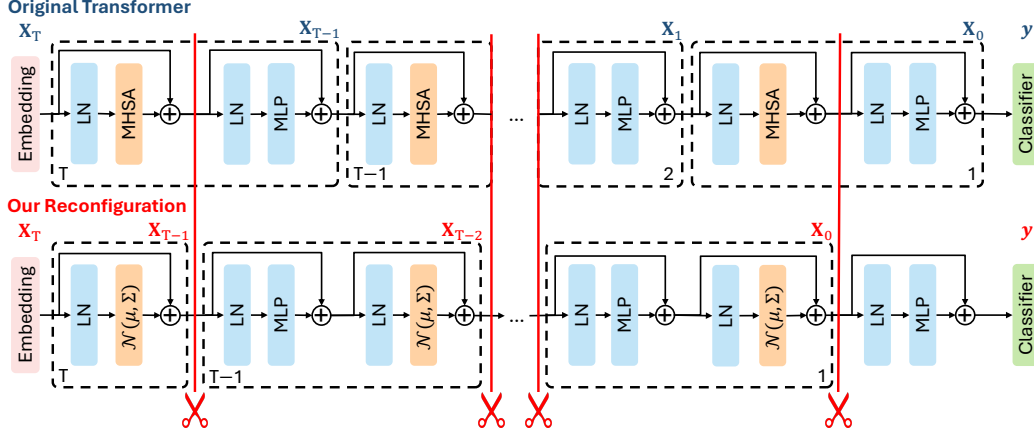


Figure 2: Restructuring a pre-trained transformer such that each block outputs a Gaussian distribution over its intermediate features, effectively aligning its architecture with a probabilistic path.

The individual output representation $F_t^{(h)}$ of each attention head h of the t -th MHSA block can then be aggregated via a linear combination O_t which preserves the (neuralized) Gaussian structure:

$$R_t = O_t [F_t^{(1)}, F_t^{(2)}, \dots, F_t^{(n)}] \Rightarrow R_t | U_t \sim \mathbb{N}(\bar{m}_t(U_t), \bar{\sigma}_t(U_t)), \quad (2)$$

where $\bar{m}_t(U_t) \triangleq [O_t \bar{m}_t^{(1)}(U_t), \dots, O_t \bar{m}_t^{(n)}(U_t)]$ and $\bar{\sigma}_t(U_t) \triangleq \text{blkdiag}[O_t \bar{\sigma}_t^{(h)}(U_t) O_t^\top]$.

This reparameterization thus reconfigures a pre-trained (point-estimate) MHSA block into probabilistic transition function with a uncertainty structure which can be optimized as in previous methods [12, 9, 15]. This provides a principled handle for uncertainty calibration. One can assess the local representation uncertainty via the (learned) predictive variance or generate uncertainty-aware representation samples to propagate downstream. This propagation is however disrupted in existing approaches as mentioned previously due to the interleaving of MHSA with point-estimated components such as MLPs and layer normalization (LN). To elaborate, the transformation from one intermediate representation X_{t-1} to the next X_t interleaves the MHSA mechanism with the MLP and LN mechanisms:

$$X_{t-1} = \text{MLP}(\text{LN}(Z_t)) + Z_t \quad \text{where} \quad Z_t = \text{MHSA}(\text{LN}(X_t)) + X_t, \quad (3)$$

where we number transformer block in reverse such that the first transformer block is indexed with $t = T$ and the last is indexed with $t = 1$, as illustrated in the upper part of Fig. 2

To propagate uncertainty under this partition, the point-estimated network segment $\text{MLP}(\text{LN}(Z_t))$ can be viewed as an observed function sampled from some function prior. However, unlike the MHSA which can be viewed as a sampled function from a learnable Gaussian process (GP) prior as established in prior works, it remains unclear how to parameterize and learn a function prior for $\text{MLP}(\text{LN}(Z_t))$ without the risk of prior misspecification. Otherwise, treating it as a deterministic transition collapses the uncertainty structure and consequently disrupts uncertainty propagation.

To sidestep this technical challenge, we propose to instead view $\text{MLP}(\text{LN}(Z_t))$ as an additional parameterization of the neuralized Gaussian transition induced by the GP-reparameterized MHSA. This can be achieved via a rearrangement of transformer's computation blocks as detailed below:

$$X_{t-1} = \text{MHSA}(\text{LN}(Z_t)) + Z_t \quad \text{where} \quad Z_t = \begin{cases} \text{MLP}(\text{LN}(X_t)) + X_t, & \text{if } t \neq T \\ X_T, & \text{otherwise} \end{cases}. \quad (4)$$

This reconfiguration guarantees that each re-partitioned computation block terminates with an MHSA module (see the lower part of Fig. 2). The deterministic transition $\text{MLP}(\text{LN}(Z_t))$ now become additional parameters of the MHSA which can be reparameterized into a neuralized Gaussian transition. Note that the skip connection does not break Gaussianity but only shifts the mean. Consequently, this construction induces a stochastic process $\{X_t\}_{t=0}^T$ with Gaussian transitions:

$$p(X_{t-1} | X_t) = \mathbb{N}(X_{t-1} | m_t(X_t), \sigma_t(X_t)), \quad (5)$$

where $m_t(\mathbf{X}_t) = \bar{m}_t(\text{LN}(\mathbf{Z}_t)) + \mathbf{Z}_t$ and $\sigma_t(\mathbf{X}_t) = \bar{\sigma}_t(\text{LN}(\mathbf{Z}_t))$ with \mathbf{Z}_t is defined in Eq. 4. These separately parameterized Gaussian transitions across timesteps can be distilled into a unified spatiotemporal Gaussian transition that defines the reverse-time process of a diffusion model as discussed in Section 2.2. This unified parameterization enables seamless uncertainty propagation while explicitly encoding transition correlations across steps as desired.

Remark. We note that the above reconfiguration does not alter the pre-trained computation, but changes how the point-estimated segment $\text{MLP}(\text{LN}(\mathbf{Z}_t))$ is interpreted. Instead of being treated as an observed function drawn from an unknown prior, it is parameterized as part of a Gaussian transition, revealing a learnable representation that is more amenable to uncertainty propagation. For brevity, we also abuse the notation \mathbf{X}/F to denote $\text{vec}(\mathbf{X})/\text{vec}(F)$.

2.2 Distilling Transformer-based Probability Path on Diffusion Model

Under our proposed reconfiguration in Section 2.1, the transformer induces a stochastic path $\{\mathbf{X}_t\}_{t=0}^T$ with Gaussian transitions (Eq. 5), which closely resembles a reverse diffusion process. This defines a distribution over intermediate features conditioned on the original input embedding \mathbf{X}_T :

$$p(\mathbf{X}_{T-1}, \dots, \mathbf{X}_0 | \mathbf{X}_T) = \prod_{t=1}^T p(\mathbf{X}_{t-1} | \mathbf{X}_t) = \prod_{t=1}^T \mathbb{N}(\mathbf{X}_{t-1} | m_t(\mathbf{X}_t), \sigma_t(\mathbf{X}_t)), \quad (6)$$

where the transition probability $p(\mathbf{X}_{t-1} | \mathbf{X}_t)$ is modeled independently at each timestep. Calibrating uncertainty in this block-wise, decoupled structure is difficult as it does not capture transition correlation and hence does not generalize across timesteps.

To address this limitation, we require a more parsimonious representation that characterizes the entire sequence of transition models in a unified manner. This can be achieved by re-compiling it into a reverse-time diffusion process with a unified spatiotemporal transition model:

$$q_\theta(\mathbf{X}_{T-1}, \dots, \mathbf{X}_0 | \mathbf{X}_T) = \prod_{t=1}^T q_\theta(\mathbf{X}_{t-1} | \mathbf{X}_t) = \prod_{t=1}^T \mathbb{N}(\mathbf{X}_{t-1} | m_\theta(\mathbf{X}_t), \sigma_\theta(\mathbf{X}_t)), \quad (7)$$

In particular, the entire sequence of neuralized Gaussian transitions derived from the previously described GP-reparameterized of pre-trained transformer can be absorbed into the reverse-time diffusion with a unified spatiotemporal transition via minimizing the following negative log-likelihood, analogous to score matching in diffusion models [57, 28]:

$$L(\theta) = \mathbb{E}_{p(\mathbf{X}_0 | \mathbf{X}_T)} \left[-\log q_\theta(\mathbf{X}_0 | \mathbf{X}_T) \right]. \quad (8)$$

This negative log-likelihood (NLL) loss admits the following upper-bound via variational inference:

$$L(\theta) \leq \mathbb{H}(p(\mathbf{X}_0 | \mathbf{X}_T)) + \sum_{t=1}^T \mathbb{E}_{p(\mathbf{X}_t | \mathbf{X}_T)} \left[D_{\text{KL}}(p(\mathbf{X}_{t-1} | \mathbf{X}_t) \| q_\theta(\mathbf{X}_{t-1} | \mathbf{X}_t)) \right], \quad (9)$$

with proof deferred to Appendix A.4. Since the entropy term $\mathbb{H}(p(\mathbf{X}_0 | \mathbf{X}_T))$ is independent of θ , optimizing the bound in Eq. 9 reduces to minimizing the Kullback-Leibler (KL) divergence:

$$L_1(\theta) = \mathbb{E}_{t \sim \mathbb{U}(1, T)} \mathbb{E}_{\mathbf{X}_t \sim p(\mathbf{X}_t | \mathbf{X}_T)} \left[D_{\text{KL}}(p(\mathbf{X}_{t-1} | \mathbf{X}_t) \| q_\theta(\mathbf{X}_{t-1} | \mathbf{X}_t)) \right], \quad (10)$$

where $t \sim \mathbb{U}(1, T)$ and \mathbf{X}_t is sampled via sampling data \mathbf{X} and simulating the corresponding output of the $(T-t)$ -th block of the pre-trained transformer. This loss aligns the probability path with a diffusion-style transition kernel while enabling generalization across timesteps. To ensure that the learned uncertainty propagation process maps from data to feature distributions which are informative for downstream prediction, we regularize it with an additional performance loss:

$$L_2(\theta) = \mathbb{E}_{(\mathbf{X}, \mathbf{y}) \sim \mathcal{D}} \mathbb{E}_{\mathbf{X}_0 \sim q_\theta(\mathbf{X}_0 | \mathbf{X}_T)} \left[\text{loss}(\mathbf{X}_0, \mathbf{y}) \right], \quad (11)$$

where \mathbf{X} is sampled from the training dataset \mathcal{D} and is embedded with $\mathbf{X}_T = \text{embed}(\mathbf{X})$. \mathbf{X}_0 is then sampled via iteratively simulating the current estimate of the probability path $q_\theta(\mathbf{X}_{t-1} | \mathbf{X}_t)$. The parameterization of the unified spatiotemporal transition model can then be obtained via:

$$\theta = \arg \min_{\theta} \left\{ L_1(\theta) + L_2(\theta) \right\}, \quad (12)$$

which combines the uncertainty-aware (reconfiguration) loss with the performance-aware loss. For implementation details of the above algorithm, please refer to Appendix A.5.

3 Experiments

This section evaluates the efficacy of our proposed method, DIRECTOR: **D**iffusion-**I**nspired **R**Econfiguration of **T**ransf**O**rmers for Uncertainty Calibration, by reconfiguring existing uncertainty-aware transformers into diffusion-based models and comparing their uncertainty calibration and predictive performance against those of the original versions. We describe our experiment settings in Section 3.1 and report detailed empirical results in Section 3.2.

3.1 Experiment Settings

Datasets. We evaluate DIRECTOR using datasets in computer vision (CV) and natural language processing (NLP). In CV, we use the CIFAR-10 and CIFAR-100 datasets [32]. Each dataset contains 45,000 training, 5000 validation, and 10,000 test images. In NLP, we use the IMDB dataset [39], with 20,000 training, 5,000 validation, and 25,000 test samples; and the CoLA dataset [69], with 6,355 training, 907 validation, and 1,816 test samples.

Baselines. We compare DIRECTOR with various uncertainty-aware baselines: Temperature Scaling (TS) [22], Monte Carlo Dropout (MCD) [21], Stochastic Variational Deep Kernel Learning (SV-DKL) [71], Kronecker-Factored Last-Layer Laplace Approximation (KFLLA) [31], Sparse Gaussian Process Attention (SGPA) [12], and Kernel-Eigen Pair Sparse Variational Gaussian Processes Attention (KEP-SVGP or KEP for brevity) [15].

Pre-Trained Models. We conduct our uncertainty-aware reconfiguration experiments on two pre-trained architectures which include (i) vanilla transformer-based model and (ii) uncertainty-aware transformer KEP [14]. For each architecture, we pre-train a 7-layer vision transformer (ViT [18]) for experiments on CIFAR-10 and CIFAR-100, and a 5-layer transformer [66] for CoLA and IMDB. We also evaluate variants of uncertainty-aware transformer KEP [14], where the first $n - k$ attention blocks use standard MHSA and the last k blocks use GP-reparameterized attention; we denote this variant as KEP- k/n .

Unified Transition Model. We implement the unified spatiotemporal transition model in our diffusion-based reparameterization using a single-block DiT [45], with embedding dimensions matched to the pre-trained models (see Appendix A.6.13 for full hyperparameters). The model is designed to be smaller than the original backbone for improved memory efficiency, containing only 2.7M parameters versus 6.24M in ViT for vision tasks, and 2.59M versus 3.38M in the text transformer for NLP tasks. Results for alternative transition model architectures are reported in Appendix A.6.7.

Evaluation Metrics. For in-distribution classification, we evaluate predictive performance using accuracy (ACC) for CIFAR-10, CIFAR-100, and IMDB, and Matthew’s Correlation Coefficient (MCC) for CoLA. Calibration is assessed with Negative Log-Likelihood ($NLL \times 10$), Expected Calibration Error (ECE %), and Brier Score (%). Failure prediction is measured using Area Under the Risk-Coverage Curve (AURC %), Area Under the Receiver Operating Characteristic Curve (AUROC %), and False Positive Rate at 95% True Positive Rate (FPR95 %). For out-of-distribution (OOD) robustness, the same metrics are applied to the CIFAR-10-C and CoLA-OOD datasets. OOD detection performance is quantified using AUROC % and Area Under the Precision-Recall Curve (AUPR %). All metrics are reported as mean \pm standard error over five runs. All experiments are conducted on 8 NVIDIA L40 GPUs.

3.2 Results and Discussion

3.2.1 In-Distribution Classification

Comparison with Pre-Trained Models. DIRECTOR demonstrates superior performance compared to pre-trained models across nearly all tasks and metrics (Table 1). On CIFAR-10, DIRECTOR outperforms KEP-7/7 on every reported metric, with higher accuracy (84.74% versus 82.68%), lower ECE (5.18 versus 6.95), lower NLL (4.84 versus 5.89), and a lower Brier score (22.48 versus 25.90), while also leading in the failure-prediction metrics. On CIFAR-100, although DIRECTOR does not outperform KEP-7/7 in ECE (21.43 versus 21.31), the difference is marginal ($< 0.2\%$), while DIRECTOR achieves significantly higher accuracy (60.85% versus 57.06%) and a lower Brier score. Additionally, significance testing, reported in Appendix A.6.8, indicates that most improvements are statistically significant (p -value < 0.05). These results demonstrate that DIRECTOR not only

Table 1: Performance comparison between pre-trained transformers and their diffusion-inspired reconfiguration using DIRECTOR on in-distribution classification tasks. KEP- k/n denotes a pre-trained transformer using GP-reparameterized architecture (KEP [15]) for the last k attention blocks and standard MHSA for the remaining blocks. Better results are shown in **bold**.

Dataset	Method	ACC/MCC \uparrow	AURC \downarrow	AUROC \uparrow	FPR95 \downarrow	ECE \downarrow	NLL \downarrow	Brier \downarrow
CIFAR-10	ViT	83.84 \pm 0.09	4.05 \pm 0.11	86.42 \pm 0.37	67.13 \pm 1.98	12.51 \pm 0.20	10.91 \pm 0.39	28.03 \pm 0.15
	DIRECTOR	85.67 \pm 0.88	3.10 \pm 0.45	87.90 \pm 1.04	61.92 \pm 1.85	9.67 \pm 0.62	6.94 \pm 0.52	23.54 \pm 1.46
	KEP-1/7	84.52 \pm 0.25	3.52 \pm 0.11	87.52 \pm 0.27	65.14 \pm 1.27	10.93 \pm 0.26	8.21 \pm 0.15	25.80 \pm 0.40
	DIRECTOR	86.51 \pm 0.57	2.78 \pm 0.16	88.28 \pm 0.16	61.85 \pm 1.93	8.61 \pm 0.49	6.11 \pm 0.27	21.90 \pm 0.82
	KEP-7/7	82.68 \pm 0.12	4.46 \pm 0.05	85.71 \pm 0.34	66.90 \pm 1.78	6.95 \pm 0.36	5.89 \pm 0.11	25.90 \pm 0.23
	DIRECTOR	84.74 \pm 0.40	3.47 \pm 0.18	87.34 \pm 0.33	62.88 \pm 1.20	5.18 \pm 0.33	4.84 \pm 0.11	22.48 \pm 0.53
CIFAR-100	ViT	52.94 \pm 0.63	22.88 \pm 0.64	81.07 \pm 0.56	75.96 \pm 2.39	30.73 \pm 0.61	32.71 \pm 0.91	74.72 \pm 1.20
	DIRECTOR	57.79 \pm 0.57	18.58 \pm 0.37	82.60 \pm 0.11	71.50 \pm 1.42	22.31 \pm 0.49	22.16 \pm 0.36	62.57 \pm 0.85
	KEP-1/7	55.74 \pm 0.77	20.20 \pm 0.64	82.10 \pm 0.20	73.82 \pm 0.92	27.07 \pm 0.71	27.45 \pm 0.62	68.54 \pm 1.18
	DIRECTOR	58.78 \pm 1.52	17.63 \pm 1.08	82.99 \pm 0.41	71.40 \pm 1.24	21.17 \pm 1.03	21.15 \pm 0.93	60.96 \pm 1.73
	KEP-7/7	57.06 \pm 0.56	19.38 \pm 0.60	82.02 \pm 0.39	72.78 \pm 0.69	21.31 \pm 3.85	22.41 \pm 2.29	63.07 \pm 2.11
	DIRECTOR	60.85 \pm 2.98	16.35 \pm 2.34	82.91 \pm 0.67	71.46 \pm 1.43	21.43 \pm 2.09	20.55 \pm 2.42	58.91 \pm 4.63
IMDB	Transformer	85.59 \pm 0.50	4.73 \pm 0.32	80.75 \pm 0.55	75.45 \pm 1.10	6.96 \pm 2.05	3.95 \pm 0.44	22.28 \pm 1.26
	DIRECTOR	86.07 \pm 0.61	4.57 \pm 0.39	80.84 \pm 0.67	74.24 \pm 0.87	5.40 \pm 1.90	3.60 \pm 0.34	21.08 \pm 1.32
	KEP-1/5	85.76 \pm 0.71	4.54 \pm 0.42	81.02 \pm 0.70	74.87 \pm 0.87	5.51 \pm 2.94	3.79 \pm 0.51	21.62 \pm 1.42
	DIRECTOR	87.13 \pm 0.19	4.07 \pm 0.30	81.55 \pm 0.62	73.35 \pm 0.14	3.16 \pm 2.54	3.24 \pm 0.31	19.31 \pm 0.97
	KEP-5/5	84.57 \pm 0.81	5.48 \pm 0.60	79.32 \pm 1.25	77.03 \pm 1.48	7.83 \pm 3.28	5.17 \pm 2.13	24.23 \pm 2.56
	DIRECTOR	85.74 \pm 0.34	4.58 \pm 0.23	80.95 \pm 0.42	75.08 \pm 1.15	2.33 \pm 1.54	3.36 \pm 0.12	20.70 \pm 0.65
CoLA	Transformer	29.92 \pm 1.17	20.80 \pm 1.21	64.22 \pm 1.46	90.01 \pm 2.84	26.44 \pm 1.90	19.66 \pm 4.18	55.09 \pm 2.68
	DIRECTOR	31.85 \pm 2.46	19.74 \pm 1.62	64.52 \pm 1.71	89.52 \pm 3.61	23.94 \pm 0.49	14.29 \pm 3.01	50.82 \pm 1.19
	KEP-1/5	30.86 \pm 2.03	19.86 \pm 2.04	65.18 \pm 1.83	89.10 \pm 2.60	24.98 \pm 2.08	16.28 \pm 4.35	52.86 \pm 2.88
	DIRECTOR	31.84 \pm 1.88	19.42 \pm 1.83	65.54 \pm 1.78	90.37 \pm 0.89	13.77 \pm 6.58	8.26 \pm 3.75	43.54 \pm 3.65
	KEP-5/5	29.28 \pm 1.21	20.82 \pm 1.98	64.47 \pm 0.90	89.65 \pm 1.04	18.95 \pm 5.66	11.83 \pm 7.96	48.65 \pm 5.84
	DIRECTOR	32.05 \pm 1.56	18.69 \pm 1.39	64.71 \pm 1.37	89.53 \pm 1.67	12.88 \pm 5.74	7.68 \pm 1.70	42.20 \pm 2.50

provides better-calibrated uncertainty estimates but also enhances predictive accuracy, underscoring the effectiveness of our propagation-based model for UC.

Comparison with Existing Uncertainty-Aware Baselines. Beyond vanilla pre-trained models, DIRECTOR also surpasses other uncertainty-aware approaches in both predictive performance and uncertainty calibration across multiple tasks (Table 2). For a fair comparison, DIRECTOR and KEP are configured with optimal settings and evaluated against standard baselines. Overall, DIRECTOR achieves the **highest** performance in 20/28 settings (across 4 datasets and 7 UC/performance metrics) and the **second-highest** in 6/28 settings, establishing a new state-of-the-art in UC.

3.2.2 Distribution Shift Robustness

We also assess both the uncertainty calibration and predictive performance of DIRECTOR in scenarios with distribution shifts in both image classification and linguistic acceptability tasks. For vision, we use the CIFAR-10-C dataset, which includes 15 corruption types (e.g., noise, blur) at 5 severity levels [25]. For language, we use the CoLA OOD dataset, which assesses novel linguistic structures [69]. On CIFAR-10-C (see Table 3), DIRECTOR substantially improves the robustness of KEP-7/7 in predictive accuracy and Brier score, while remaining comparable in ECE and NLL under distribution shift. It also remains competitive with ViT and KEP-1/7 in predictive performance while improving on calibration metrics. On CoLA OOD (see Table 4), DIRECTOR significantly improves calibration metrics without sacrificing MCC, except when compared to KEP-5/5 which has slightly better MCC but is weaker on UC metrics. These observations consistently demonstrate both the performance robustness and generalization capability of DIRECTOR under scenarios with distribution shifts.

3.2.3 Out-of-Distribution Detection

Uncertainty-aware baselines can also be evaluated in terms of their abilities to distinguish between (i) correctly classified in-distribution samples, (ii) misclassified in-distribution samples, and (iii) out-of-distribution (OOD) samples. To assess this capability, we report the average performance with standard error of DIRECTOR in a number of OOD detection scenarios (see Table 5) using the AUROC/AUPR metrics and two standard methods: (1) Maximum Softmax Probability [26] and

Table 2: Comparison of average performance achieved by the diffusion-based reconfigured KEP [15] produced by DIRECTOR and other uncertainty-aware baselines on in-distribution classification tasks. **Blue** marks the best result across all baselines for a dataset while **brown** denotes the second-best. \uparrow indicates that higher values are better, while \downarrow indicates that lower values are better.

Dataset	Method	ACC/MCC \uparrow	AURC \downarrow	AUROC \uparrow	FPR95 \downarrow	ECE \downarrow	NLL \downarrow	Brier \downarrow
CIFAR-10	TS	83.84 \pm 0.09	3.88 \pm 0.10	86.82 \pm 0.37	65.99 \pm 1.94	9.22 \pm 0.36	6.58 \pm 0.16	25.50 \pm 0.13
	MCD	84.06 \pm 0.23	8.65 \pm 0.03	86.51 \pm 0.32	66.15 \pm 0.60	9.47 \pm 0.16	8.36 \pm 0.32	25.45 \pm 0.29
	KFLLA	83.84 \pm 0.10	3.91 \pm 0.11	86.71 \pm 0.45	65.44 \pm 1.58	8.18 \pm 0.80	6.09 \pm 0.40	24.98 \pm 0.59
	SV-DKL	83.23 \pm 0.17	4.39 \pm 0.18	85.94 \pm 0.36	66.96 \pm 1.30	11.64 \pm 0.81	9.85 \pm 1.09	27.97 \pm 0.77
	SGPA	75.59 \pm 3.63	8.41 \pm 2.37	82.65 \pm 1.71	71.78 \pm 2.73	1.92 \pm 0.55	7.11 \pm 0.95	33.98 \pm 4.57
	ViT	83.84 \pm 0.09	4.05 \pm 0.11	86.42 \pm 0.37	67.13 \pm 1.98	12.51 \pm 0.20	10.91 \pm 0.39	28.03 \pm 0.15
	KEP	84.52 \pm 0.25	3.52 \pm 0.11	87.52 \pm 0.27	65.14 \pm 1.27	10.93 \pm 0.26	8.21 \pm 0.15	25.80 \pm 0.40
DIRECTOR	84.74 \pm 0.40	3.47 \pm 0.18	87.34 \pm 0.33	62.88 \pm 1.20	5.18 \pm 0.33	4.84 \pm 0.11	22.48 \pm 0.53	
CIFAR-100	TS	52.94 \pm 0.63	22.34 \pm 0.61	82.29 \pm 0.48	71.65 \pm 1.98	17.06 \pm 0.42	21.57 \pm 0.52	64.77 \pm 0.95
	MCD	53.49 \pm 0.62	22.24 \pm 0.56	81.60 \pm 0.19	73.02 \pm 0.51	25.93 \pm 0.37	29.24 \pm 0.73	70.02 \pm 0.92
	KFLLA	52.27 \pm 0.86	23.96 \pm 0.78	81.30 \pm 0.48	71.42 \pm 1.92	18.52 \pm 5.40	20.89 \pm 0.57	66.51 \pm 1.66
	SV-DKL	51.03 \pm 0.60	24.38 \pm 0.43	81.32 \pm 0.50	73.99 \pm 1.40	25.46 \pm 0.72	28.93 \pm 0.66	71.90 \pm 0.74
	SGPA	52.77 \pm 0.52	22.84 \pm 0.52	81.65 \pm 0.36	72.02 \pm 1.74	10.33 \pm 2.25	19.10 \pm 0.57	62.08 \pm 1.04
	ViT	52.94 \pm 0.63	22.88 \pm 0.64	81.07 \pm 0.56	75.96 \pm 2.39	30.73 \pm 0.61	32.71 \pm 0.91	74.72 \pm 1.20
	KEP	57.06 \pm 0.56	19.38 \pm 0.60	82.02 \pm 0.39	72.78 \pm 0.69	21.31 \pm 3.85	22.41 \pm 2.29	63.07 \pm 2.11
DIRECTOR	60.85 \pm 2.98	16.35 \pm 2.34	82.91 \pm 0.67	71.46 \pm 1.43	21.43 \pm 2.09	20.55 \pm 2.42	58.91 \pm 4.63	
IMDB	TS	85.59 \pm 0.50	4.73 \pm 0.32	80.75 \pm 0.55	75.45 \pm 1.10	2.91 \pm 1.51	3.41 \pm 0.13	21.04 \pm 0.74
	MCD	85.96 \pm 0.42	4.40 \pm 0.24	81.40 \pm 0.55	74.79 \pm 0.88	4.18 \pm 2.03	3.47 \pm 0.23	20.72 \pm 0.82
	KFLLA	85.59 \pm 0.50	4.71 \pm 0.30	80.82 \pm 0.48	75.45 \pm 1.11	5.84 \pm 2.21	6.93 \pm 0.00	21.86 \pm 1.19
	SV-DKL	85.69 \pm 0.66	5.58 \pm 0.79	78.54 \pm 2.20	75.32 \pm 0.84	8.52 \pm 1.57	4.49 \pm 0.65	23.10 \pm 1.66
	SGPA	85.39 \pm 0.36	4.96 \pm 0.49	80.04 \pm 1.14	76.44 \pm 0.96	6.04 \pm 1.71	3.96 \pm 0.50	22.19 \pm 1.06
	Transformer	85.59 \pm 0.50	4.73 \pm 0.32	80.75 \pm 0.55	75.45 \pm 1.10	6.96 \pm 2.05	3.95 \pm 0.44	22.28 \pm 1.26
	KEP	85.76 \pm 0.71	4.54 \pm 0.42	81.02 \pm 0.70	74.87 \pm 0.87	5.51 \pm 2.94	3.79 \pm 0.51	21.62 \pm 1.42
DIRECTOR	87.13 \pm 0.19	4.07 \pm 0.30	81.55 \pm 0.62	73.35 \pm 0.14	3.16 \pm 2.54	3.24 \pm 0.31	19.31 \pm 0.97	
CoLA	TS	29.92 \pm 1.17	20.84 \pm 1.23	64.31 \pm 1.44	89.93 \pm 2.95	23.22 \pm 2.99	11.04 \pm 1.91	51.70 \pm 3.42
	MCD	30.04 \pm 1.02	20.66 \pm 1.11	64.53 \pm 1.00	89.51 \pm 1.35	24.96 \pm 1.79	17.83 \pm 3.61	53.52 \pm 2.59
	KFLLA	29.89 \pm 1.14	20.82 \pm 1.26	64.22 \pm 1.46	89.87 \pm 3.24	24.36 \pm 2.25	12.16 \pm 1.49	52.80 \pm 2.85
	SV-DKL	30.07 \pm 1.41	22.76 \pm 2.28	61.98 \pm 3.09	89.00 \pm 2.55	25.71 \pm 1.60	17.96 \pm 3.26	54.40 \pm 2.13
	SGPA	31.53 \pm 2.05	20.44 \pm 2.60	64.34 \pm 1.95	90.79 \pm 0.87	26.22 \pm 1.51	28.65 \pm 7.23	54.08 \pm 2.44
	Transformer	29.92 \pm 1.17	20.80 \pm 1.21	64.22 \pm 1.46	90.01 \pm 2.84	26.44 \pm 1.90	19.66 \pm 4.18	55.09 \pm 2.68
	KEP	30.86 \pm 2.03	19.86 \pm 2.04	65.18 \pm 1.83	89.10 \pm 2.60	24.98 \pm 2.08	16.28 \pm 4.35	52.86 \pm 2.88
DIRECTOR	32.05 \pm 1.56	18.69 \pm 1.39	64.71 \pm 1.37	89.53 \pm 1.67	12.88 \pm 5.74	7.68 \pm 1.70	42.20 \pm 2.50	

Table 3: Comparison on CIFAR10-C.

Method	ACC \uparrow	ECE \downarrow	NLL \downarrow	Brier \downarrow
ViT	69.67 \pm 0.34	24.30 \pm 0.31	23.59 \pm 1.00	53.07 \pm 0.59
DIRECTOR	68.89 \pm 1.44	22.32 \pm 1.09	17.71 \pm 1.02	51.77 \pm 2.39
KEP-1/7	69.87 \pm 0.45	22.12 \pm 0.47	18.54 \pm 0.63	50.65 \pm 0.90
DIRECTOR	69.29 \pm 0.66	20.98 \pm 0.65	16.23 \pm 0.60	50.07 \pm 1.20
KEP-7/7	59.57 \pm 0.30	21.78 \pm 0.59	17.17 \pm 0.39	60.67 \pm 0.72
DIRECTOR	68.12 \pm 0.26	22.19 \pm 0.19	17.70 \pm 0.17	52.27 \pm 0.35

Table 4: Comparison on CoLA OOD.

Method	MCC \uparrow	ECE \downarrow	NLL \downarrow	Brier \downarrow
Transformer	18.43 \pm 3.55	31.99 \pm 2.70	23.82 \pm 5.16	65.50 \pm 4.32
DIRECTOR	23.06 \pm 4.69	28.72 \pm 1.87	17.18 \pm 3.75	59.91 \pm 2.20
KEP-1/5	19.44 \pm 1.94	30.33 \pm 1.48	19.67 \pm 4.82	61.97 \pm 2.25
DIRECTOR	22.10 \pm 5.49	17.50 \pm 7.52	9.34 \pm 4.50	49.92 \pm 5.80
KEP-5/5	21.14 \pm 3.48	23.27 \pm 6.61	14.25 \pm 10.66	55.12 \pm 7.78
DIRECTOR	20.20 \pm 5.46	17.49 \pm 5.93	8.61 \pm 1.99	48.55 \pm 3.67

Entropy Maximization [10]. Using CIFAR-10 as the in-distribution dataset, our evaluation on SVHN, CIFAR-100, and LSUN demonstrates that the performance of most pre-trained transformer (using CIFAR-100 data) in most cases can be substantially improved by their corresponding diffusion-based reconfiguration. Notably, the diffusion-inspired reconfiguration of KEP-2/7 produced by DIRECTOR outperforms all baselines as highlighted in **blue**.

Additional results, including large-scale experiments on ViT-B-16 (86M) and Qwen-2.5 (494M), deep ensembles [33], reconfiguration of the SGPA backbone, post-hoc Temperature Scaling applied to every baseline, computational and memory overhead, and loss component ablations are provided in Appendix A.6.

4 Related Work

In safety-critical decision-making applications (e.g., healthcare [1, 38, 5]), models must recognize when their confidence is low to defer decisions to human experts [46, 64]. However, existing transformers typically ignore uncertainty due to point-estimate designs throughout their stack of neural transformations [44]. Prior investigation in Bayesian deep learning (BDL) are often restricted

Table 5: Comparison of average OOD detection performance in AUROC (%) and AUPR (%) (with reported standard error) achieved by the tested baselines over 5 independent runs.

Method	SVHN		CIFAR-100		LSUN	
	AUROC \uparrow	AUPR \uparrow	AUROC \uparrow	AUPR \uparrow	AUROC \uparrow	AUPR \uparrow
MCD	87.09 \pm 8.53	91.46 \pm 4.87	76.27 \pm 0.35	78.82 \pm 0.41	88.41 \pm 2.05	91.19 \pm 1.51
KFLLA	89.47 \pm 9.07	92.92 \pm 5.27	77.27 \pm 0.42	79.88 \pm 0.42	90.77 \pm 2.93	92.61 \pm 2.24
SVDKL	86.59 \pm 6.86	90.78 \pm 4.04	75.99 \pm 0.74	77.89 \pm 1.23	87.81 \pm 2.52	90.60 \pm 1.91
SGPA	61.57 \pm 5.11	74.59 \pm 3.50	73.42 \pm 1.87	75.93 \pm 1.87	67.34 \pm 9.77	76.76 \pm 5.93
ViT	87.09 \pm 8.53	91.46 \pm 4.87	76.27 \pm 0.35	78.82 \pm 0.41	88.41 \pm 2.05	91.19 \pm 1.51
DIRECTOR	83.19 \pm 10.94	88.84 \pm 6.37	78.57 \pm 0.94	81.33 \pm 0.95	83.97 \pm 7.19	88.70 \pm 4.50
KEP-1/7	75.28 \pm 19.12	81.92 \pm 13.36	77.93 \pm 0.39	80.85 \pm 0.46	85.64 \pm 4.47	88.98 \pm 3.57
DIRECTOR	90.73 \pm 4.07	93.21 \pm 2.78	79.29 \pm 0.50	82.11 \pm 0.40	89.38 \pm 3.22	92.08 \pm 2.37
KEP-2/7	88.25 \pm 4.67	91.56 \pm 3.14	77.71 \pm 0.55	80.58 \pm 0.53	88.35 \pm 3.62	91.18 \pm 2.75
DIRECTOR	92.14 \pm 5.70	94.49 \pm 3.59	79.43 \pm 0.57	82.15 \pm 0.57	91.39 \pm 2.74	93.63 \pm 1.86
KEP-7/7	77.16 \pm 1.62	84.09 \pm 1.28	76.21 \pm 0.41	78.82 \pm 0.41	77.01 \pm 3.28	82.42 \pm 2.73
DIRECTOR	79.33 \pm 20.83	85.92 \pm 13.88	79.11 \pm 0.39	81.70 \pm 0.38	86.84 \pm 4.07	90.05 \pm 3.16

to moderate-sized DL architectures [68, 42, 30, 24, 16, 52, 62, 20, 61, 53, 47], limiting scalability to large networks [44]. To elaborate, we next discuss two main UC paradigms:

UC integration during training. These methods treat model parameters as random variables and learn their posterior distributions conditioned on data. Bayesian neural networks approximate posteriors via MCMC or variational inference [6, 23], while deep ensembles [33] approximate them non-parametrically through diverse initializations. Evidential methods [72, 56] map features to prior parameters over the likelihood for a closed-form uncertainty estimation via conjugate priors. Sampling-based methods offer higher fidelity by avoiding structural assumptions but incur prohibitive sampling cost for large models [70]. In contrast, variational and evidential approaches are more scalable but less accurate due to biased approximations and restrictive parameterizations [73, 11]. Overall, these approaches approximate or sample from the parameter posterior, which remains highly intractable and often yields unreliable estimates.

UC integration post-training. These methods recalibrate prediction confidence by augmenting a trained model’s output without altering most its parameters, including data augmentation [67], Monte Carlo dropout [21], and input-gradient norms [3]. There are also learning-based approaches that adjust output probabilities to better reflect correctness, such as temperature scaling [22], replacing the solution head with probabilistic alternatives (e.g., Gaussian processes [51], SNGPs [36, 7]), or Laplace approximation that fits a local Gaussian approximation to the weight posterior around the model’s learned parameters [34]. More recently, conformal prediction [40] offers a black-box calibration method that uses a pre-trained model’s softmax scores and test-time data to produce prediction sets with marginal coverage guarantees.

Uncertainty calibration versus uncertainty quantification. Beyond the uncertainty calibration methods discussed above, uncertainty quantification also plays an important role in safety-critical decision-making applications. While closely related, uncertainty calibration (UC) and uncertainty quantification (UQ) address different aspects of predictive uncertainty. UC focuses on the reliability of a model’s confidence estimates, ensuring that predicted confidence aligns with empirical correctness (e.g., predictions made with confidence p are correct approximately p fraction of the time). In contrast, UQ aims to model and represent uncertainty itself, characterizing predictive variability arising from sources such as data noise (aleatoric uncertainty) and model uncertainty (epistemic uncertainty). As a result, a model may exhibit rich uncertainty estimates but remain poorly calibrated, or be well-calibrated yet provide uninformative uncertainty. This distinction highlights that UC and UQ are complementary but non-interchangeable objectives, and motivates approaches that explicitly target calibration reliability in large-scale transformer models.

5 Conclusion

We introduce a diffusion-inspired reconfiguration of pre-trained transformers that enables principled uncertainty propagation across the entire feature transformation stack. Our approach builds on

the established connection between multi-head self-attention (MHSA) and Gaussian process (GP) prediction, reparameterizing the feature transformation stack as a sequence of neuralized Gaussian transitions. This sequence is distilled into a diffusion process with a learnable unified spatiotemporal transition model that maps between data and feature distributions, embedding expressive uncertainty-aware structure within the original transformer while preserving predictive performance. We comprehensively evaluate our method across diverse vision and language tasks, consistently demonstrating its effectiveness. These results point to a new direction for embedding probabilistic reasoning into large pre-trained models, enhancing reliability in risk-sensitive applications.

References

- [1] Shamsi A., Asgharnezhad H., and Jokandan SS. An uncertainty-aware transfer learning-based framework for covid-19 diagnosis. *IEEE Transaction on Neural Network Learning Systems*, 2021.
- [2] Josh Achiam, Steven Adler, Sandhini Agarwal, Lama Ahmad, Ilge Akkaya, Florencia Leoni Aleman, Diogo Almeida, Janko Altenschmidt, Sam Altman, Shyamal Anadkat, et al. Gpt-4 technical report. *arXiv preprint arXiv:2303.08774*, 2023.
- [3] Jordan T Ash et al. Deep batch active learning by diverse, uncertain gradient lower bounds. *arXiv preprint arXiv:1906.03671*, 2019.
- [4] Alexei Baevski, Yuhao Zhou, Abdelrahman Mohamed, and Michael Auli. wav2vec 2.0: A framework for self-supervised learning of speech representations. *Advances in neural information processing systems*, 33:12449–12460, 2020.
- [5] Neil Band, Tim G. J. Rudner, Qixuan Feng, Angelos Filos, Zachary Nado, Michael W. Dusenberry, Ghassen Jerfel, Dustin Tran, and Yarín Gal. Benchmarking bayesian deep learning on diabetic retinopathy detection tasks. *ArXiv*, abs/2211.12717, 2022.
- [6] Charles Blundell, Julien Cornebise, Koray Kavukcuoglu, and Daan Wierstra. Weight uncertainty in neural network. In *International conference on machine learning*, pages 1613–1622. PMLR, 2015.
- [7] John Bradshaw, Alexander G de G Matthews, and Zoubin Ghahramani. Adversarial examples, uncertainty, and transfer testing robustness in gaussian process hybrid deep networks. *arXiv preprint arXiv:1707.02476*, 2017.
- [8] Tom Brown, Benjamin Mann, Nick Ryder, Melanie Subbiah, Jared D Kaplan, Prafulla Dhariwal, Arvind Neelakantan, Pranav Shyam, Girish Sastry, Amanda Askell, et al. Language models are few-shot learners. *Advances in neural information processing systems*, 33:1877–1901, 2020.
- [9] Long Minh Bui, Tho Tran Huu, Duy Dinh, Tan Minh Nguyen, and Trong Nghia Hoang. Revisiting kernel attention with correlated gaussian process representation. *arXiv preprint arXiv:2502.20525*, 2025.
- [10] Robin Chan, Matthias Rottmann, and Hanno Gottschalk. Entropy maximization and meta classification for out-of-distribution detection in semantic segmentation, 2021.
- [11] Tian Chen, Jeffrey Streets, and Babak Shahbaba. A geometric view of posterior approximation. *arXiv preprint arXiv:1510.00861*, 2015.
- [12] Wenlong Chen and Yingzhen Li. Calibrating transformers via sparse gaussian processes. *arXiv preprint arXiv:2303.02444*, 2023.
- [13] Yingyi Chen, Qinghua Tao, Francesco Tonin, and Johan Suykens. Primal-attention: Self-attention through asymmetric kernel svd in primal representation. *Advances in Neural Information Processing Systems*, 36, 2024.
- [14] Yingyi Chen, Qinghua Tao, Francesco Tonin, and Johan Suykens. Self-attention through kernel-eigen pair sparse variational gaussian processes. In *Forty-first International Conference on Machine Learning*, 2024.
- [15] Yingyi Chen, Qinghua Tao, Francesco Tonin, and Johan AK Suykens. Self-attention through kernel-eigen pair sparse variational gaussian processes. *arXiv preprint arXiv:2402.01476*, 2024.
- [16] Jen-Tzung Chien and Yuan-Chu Ku. Bayesian recurrent neural network for language modeling. *IEEE transactions on neural networks and learning systems*, 27(2):361–374, 2015.
- [17] Jacob Devlin, Ming-Wei Chang, Kenton Lee, and Kristina Toutanova. Bert: Pre-training of deep bidirectional transformers for language understanding. In *Proceedings of the 2019 conference of the North American chapter of the association for computational linguistics: human language technologies, volume 1 (long and short papers)*, pages 4171–4186, 2019.

- [18] Alexey Dosovitskiy, Lucas Beyer, Alexander Kolesnikov, Dirk Weissenborn, Xiaohua Zhai, Thomas Unterthiner, Mostafa Dehghani, Matthias Minderer, Georg Heigold, Sylvain Gelly, et al. An image is worth 16x16 words: Transformers for image recognition at scale. *arXiv preprint arXiv:2010.11929*, 2020.
- [19] Danny Driess, Fei Xia, Mehdi SM Sajjadi, Corey Lynch, Aakanksha Chowdhery, Ayzaan Wahid, Jonathan Tompson, Quan Vuong, Tianhe Yu, Wenlong Huang, et al. Palm-e: An embodied multimodal language model. *arXiv preprint arXiv:2303.03378*, 2023.
- [20] Vincent Fortuin, Adrià Garriga-Alonso, Sebastian W. Ober, Florian Wenzel, Gunnar Ratsch, Richard E Turner, Mark van der Wilk, and Laurence Aitchison. Bayesian neural network priors revisited. In *International Conference on Learning Representations*, 2022.
- [21] Yarin Gal and Zoubin Ghahramani. Dropout as a bayesian approximation: Representing model uncertainty in deep learning. In *international conference on machine learning*, pages 1050–1059. PMLR, 2016.
- [22] Chuan Guo, Geoff Pleiss, Yu Sun, and Kilian Q Weinberger. On calibration of modern neural networks. In *International conference on machine learning*, pages 1321–1330. PMLR, 2017.
- [23] Hongji Guo, Hanjing Wang, and Qiang Ji. Uncertainty-guided probabilistic transformer for complex action recognition. In *Proceedings of the IEEE/CVF Conference on Computer Vision and Pattern Recognition*, pages 1935–1944, 2022.
- [24] Fredrik K Gustafsson, Martin Danelljan, and Thomas B Schon. Evaluating scalable bayesian deep learning methods for robust computer vision. In *Proceedings of the IEEE/CVF conference on computer vision and pattern recognition workshops*, pages 318–319, 2020.
- [25] Dan Hendrycks and Thomas Dietterich. Benchmarking neural network robustness to common corruptions and perturbations. *Proceedings of the International Conference on Learning Representations*, 2019.
- [26] Dan Hendrycks and Kevin Gimpel. A baseline for detecting misclassified and out-of-distribution examples in neural networks. In *International Conference on Learning Representations*, 2017.
- [27] Geoffrey Hinton, Oriol Vinyals, and Jeff Dean. Distilling the knowledge in a neural network, 2015.
- [28] Jonathan Ho, Ajay Jain, and Pieter Abbeel. Denoising diffusion probabilistic models. *Advances in Neural Information Processing Systems*, 33:6840–6851, 2020.
- [29] Wei-Ning Hsu, Benjamin Bolte, Yao-Hung Hubert Tsai, Kushal Lakhotia, Ruslan Salakhutdinov, and Abdelrahman Mohamed. Hubert: Self-supervised speech representation learning by masked prediction of hidden units. *IEEE/ACM transactions on audio, speech, and language processing*, 29:3451–3460, 2021.
- [30] Alex Kendall and Yarin Gal. What uncertainties do we need in bayesian deep learning for computer vision? *Advances in Neural Information Processing Systems*, 30, 2017.
- [31] Agustinus Kristiadi, Matthias Hein, and Philipp Hennig. Being Bayesian, even just a bit, fixes overconfidence in ReLU networks. In *International Conference on Machine Learning*, pages 5436–5446, 2020.
- [32] Alex Krizhevsky, Geoffrey Hinton, et al. Learning multiple layers of features from tiny images. *Technical Report*, 2009.
- [33] Balaji Lakshminarayanan, Alexander Pritzel, and Charles Blundell. Simple and scalable predictive uncertainty estimation using deep ensembles. *Advances in neural information processing systems*, 30, 2017.
- [34] Wanyu Li, Pengfei Sun, Yifan Liu, Junyi Li, and Yang Liu. Uncertainty quantification in deep learning: A survey. *Artificial Intelligence Review*, 2023.
- [35] Haotian Liu, Chunyuan Li, Qingyang Wu, and Yong Jae Lee. Visual instruction tuning. *Advances in neural information processing systems*, 36:34892–34916, 2023.

- [36] Jeremiah Liu, Zi Lin, Shreyas Padhy, Dustin Tran, Tania Bedrax Weiss, and Balaji Lakshminarayanan. Simple and principled uncertainty estimation with deterministic deep learning via distance awareness. *Advances in neural information processing systems*, 33:7498–7512, 2020.
- [37] Ze Liu, Yutong Lin, Yue Cao, Han Hu, Yixuan Wei, Zheng Zhang, Stephen Lin, and Baining Guo. Swin transformer: Hierarchical vision transformer using shifted windows. In *Proceedings of the IEEE/CVF international conference on computer vision*, pages 10012–10022, 2021.
- [38] L. Julian Lechuga Lopez, Tim G. J. Rudner, Farah E. Shamout, Sanyam Kapoor, Shikai Qiu, Andrew Gordon, Yiqiu Shen, Nan Wu, Aakash Kaku, Jungkyu Park, Taro Makino, Stanislaw Jastrzkeski, Jan Witowski, Duo Wang, Ben Zhang, Dustin Tran, Jeremiah Liu, Michael W. Dusenberry, Du Phan, Mark Collier, Jie Ren, Kehang Han, Zi Wang, Zelda E. Mariet, Huiyi Hu, Neil Band, Karan Singhal, Zachary Nado, Joost R. van Amersfoort, Andreas Kirsch, Rodolphe Jenat-ton, Nithum Thain, Honglin Yuan, Kelly Buchanan, Kevin Murphy, D. Sculley, Yarin Gal, Zoubin Ghahramani, Jasper Snoek, and Balaji Lakshmi-narayanan. Informative priors improve the reliability of multimodal clinical data classification. *ArXiv*, abs/2312.00794, 2023.
- [39] Andrew Maas, Raymond E Daly, Peter T Pham, Dan Huang, Andrew Y Ng, and Christopher Potts. Learning word vectors for sentiment analysis. In *Annual Meeting of the Association for Computational Linguistics: Human Language Technologies*, pages 142–150, 2011.
- [40] Charles Marx, Shengjia Zhao, Willie Neiswanger, and Stefano Ermon. Modular conformal calibration. In *Proceedings of the 39th International Conference on Machine Learning (ICML)*, 2022.
- [41] Jooyoung Moon, Jihyo Kim, Younghak Shin, and Sangheum Hwang. Confidence-aware learning for deep neural networks. In *international conference on machine learning*, pages 7034–7044. PMLR, 2020.
- [42] Jishnu Mukhoti and Yarin Gal. Evaluating bayesian deep learning methods for semantic segmentation. *arXiv preprint arXiv:1811.12709*, 2018.
- [43] Jishnu Mukhoti, Viveka Kulharia, Amartya Sanyal, Stuart Golodetz, Philip Torr, and Puneet Dokania. Calibrating deep neural networks using focal loss. *Advances in neural information processing systems*, 33:15288–15299, 2020.
- [44] Theodore Papamarkou, Maria Skoularidou, Konstantina Palla, Laurence Aitchison, Julyan Arbel, David Dunson, Maurizio Filippone, Vincent Fortuin, Philipp Hennig, Jos’e Miguel Hern’andez-Lobato, Aliaksandr Hubin, Alexander Immer, Theofanis Karaletsos, Mohammad Emteyaz Khan, Agustinus Kristiadi, Yingzhen Li, Stephan Mandt, Christopher Nemeth, Michael A. Osborne, Tim G. J. Rudner, David Rugamer, Yee Whye Teh, Max Welling, Andrew Gordon Wilson, and Ruqi Zhang. Position: Bayesian deep learning is needed in the age of large-scale AI. In *International Conference on Machine Learning*, 2024.
- [45] William Peebles and Saining Xie. Scalable diffusion models with transformers. *arXiv preprint arXiv:2212.09748*, 2022.
- [46] Tadeusz Pietraszek. On the use of ROC analysis for the optimization of abstaining classifiers. *Machine Learning*, 68:137–169, 2007.
- [47] Shikai Qiu, Tim G. J. Rudner, Sanyam Kapoor, and Andrew Gordon Wilson. Should we learn most likely functions or parameters? In *Thirty-seventh Conference on Neural Information Processing Systems*, 2023.
- [48] Alec Radford, Jong Wook Kim, Chris Hallacy, Aditya Ramesh, Gabriel Goh, Sandhini Agarwal, Girish Sastry, Amanda Askell, Pamela Mishkin, Jack Clark, et al. Learning transferable visual models from natural language supervision. In *International conference on machine learning*, pages 8748–8763. PmLR, 2021.
- [49] Alec Radford, Jong Wook Kim, Tao Xu, Greg Brockman, Christine McLeavey, and Ilya Sutskever. Robust speech recognition via large-scale weak supervision. In *International conference on machine learning*, pages 28492–28518. PMLR, 2023.

- [50] Alec Radford, Jeffrey Wu, Rewon Child, David Luan, Dario Amodei, Ilya Sutskever, et al. Language models are unsupervised multitask learners. *OpenAI blog*, 1(8):9, 2019.
- [51] Carl Edward Rasmussen and Christopher KI Williams. Gaussian processes for machine learning. *MIT press Cambridge, MA*, 1(3), 2006.
- [52] Hippolyt Ritter, Martin Kukla, Cheng Zhang, and Yingzhen Li. Sparse uncertainty representation in deep learning with inducing weights. *Advances in Neural Information Processing Systems*, 34:6515–6528, 2021.
- [53] Tim G. J. Rudner, Freddie Bickford Smith, Qixuan Feng, Yee Whye Teh, and Yarin Gal. Continual learning via sequential function-space variational inference. In Kamalika Chaudhuri, Stefanie Jegelka, Le Song, Csaba Szepesvari, Gang Niu, and Sivan Sabato, editors, *Proceedings of the 39th International Conference on Machine Learning*, volume 162 of *Proceedings of Machine Learning Research*, pages 18871–18887. PMLR, 17–23 Jul 2022.
- [54] Tim GJ Rudner, Zonghao Chen, Yee Whye Teh, and Yarin Gal. Tractable function-space variational inference in bayesian neural networks. *Advances in Neural Information Processing Systems*, 35:22686–22698, 2022.
- [55] Tim GJ Rudner, Sanyam Kapoor, Shikai Qiu, and Andrew Gordon Wilson. Function-space regularization in neural networks: A probabilistic perspective. In *International Conference on Machine Learning*, pages 29275–29290. PMLR, 2023.
- [56] Murat Sensoy, Lance Kaplan, and M R Kandemir. Evidential deep learning to quantify classification uncertainty. *arXiv preprint arXiv:1806.01768*, 2018.
- [57] Jascha Sohl-Dickstein, Eric Weiss, Niru Maheswaranathan, and Surya Ganguli. Deep unsupervised learning using nonequilibrium thermodynamics. In *International conference on machine learning*, pages 2256–2265. pmlr, 2015.
- [58] Gemini Team, Rohan Anil, Sebastian Borgeaud, Jean-Baptiste Alayrac, Jiahui Yu, Radu Soricut, Johan Schalkwyk, Andrew M Dai, Anja Hauth, Katie Millican, et al. Gemini: a family of highly capable multimodal models. *arXiv preprint arXiv:2312.11805*, 2023.
- [59] Hugo Touvron, Matthieu Cord, Matthijs Douze, Francisco Massa, Alexandre Sablayrolles, and Hervé Jégou. Training data-efficient image transformers & distillation through attention. In *International conference on machine learning*, pages 10347–10357. PMLR, 2021.
- [60] Hugo Touvron, Thibaut Lavril, Gautier Izacard, Xavier Martinet, Marie-Anne Lachaux, Timothée Lacroix, Baptiste Rozière, Naman Goyal, Eric Hambro, Faisal Azhar, et al. Llama: Open and efficient foundation language models. *arXiv preprint arXiv:2302.13971*, 2023.
- [61] Ba-Hien Tran, Simone Rossi, Dimitrios Milios, and Maurizio Filippone. All you need is a good functional prior for bayesian deep learning. *Journal of Machine Learning Research*, 23:74:1–74:56, 2020.
- [62] Dustin Tran, Mike Dusenberry, Mark Van Der Wilk, and Danijar Hafner. Bayesian layers: A module for neural network uncertainty. *Advances in neural information processing systems*, 32, 2019.
- [63] Dustin Tran, Jeremiah Liu, Michael W Dusenberry, Du Phan, Mark Collier, Jie Ren, Kehang Han, Zi Wang, Zelda Mariet, Huiyi Hu, et al. Plex: Towards reliability using pretrained large model extensions. *arXiv preprint arXiv:2207.07411*, 2022.
- [64] Dustin Tran, Jeremiah Zhe Liu, Michael W. Dusenberry, Du Phan, Mark Collier, Jie Jessie Ren, Kehang Han, Z. Wang, Zelda E. Mariet, Huiyi Hu, Neil Band, Tim G. J. Rudner, K. Singhal, Zachary Nado, Joost R. van Amersfoort, Andreas Kirsch, Rodolphe Jenatton, Nithum Thain, Honglin Yuan, E. Kelly Buchanan, Kevin Murphy, D. Sculley, Yarin Gal, Zoubin Ghahramani, Jasper Snoek, and Balaji Lakshminarayanan. Plex: Towards reliability using pretrained large model extensions. *ArXiv*, abs/2207.07411, 2022.

- [65] Yao-Hung Hubert Tsai, Shaojie Bai, Makoto Yamada, Louis-Philippe Morency, and Ruslan Salakhutdinov. Transformer dissection: a unified understanding of transformer’s attention via the lens of kernel. *arXiv preprint arXiv:1908.11775*, 2019.
- [66] Ashish Vaswani, Noam Shazeer, Niki Parmar, Jakob Uszkoreit, Llion Jones, Aidan N Gomez, Łukasz Kaiser, and Illia Polosukhin. Attention is all you need. *Advances in neural information processing systems*, 30, 2017.
- [67] Guotai Wang et al. Aleatoric uncertainty estimation with test-time augmentation for medical image segmentation with convolutional neural networks. *Neurocomputing*, 338:34–45, 2019.
- [68] Hao Wang and D. Y. Yeung. Towards bayesian deep learning: A survey. *ArXiv*, abs/1604.01662, 2016.
- [69] Alex Warstadt, Amanpreet Singh, and Samuel R Bowman. Neural network acceptability judgments. *Transactions of the Association for Computational Linguistics*, 7:625–641, 2019.
- [70] Florian Wenzel, Jonas Rothfuss, Bastiaan Veeling, Jakub Swiatkowski, Linh Tran, Stephan Mandt, Jasper Snoek, Tim Salimans, Rodolphe Jenatton, and Sebastian Nowozin. How good is the bayes posterior in deep neural networks really? In *International Conference on Machine Learning*, pages 10248–10259. PMLR, 2020.
- [71] Andrew G Wilson, Zhiting Hu, Russ R Salakhutdinov, and Eric P Xing. Stochastic variational deep kernel learning. *Advances in Neural Information Processing Systems*, 29, 2016.
- [72] Andrew Gordon Wilson, Zhiting Hu, Ruslan Salakhutdinov, and Eric P. Xing. Deep kernel learning. In Arthur Gretton and Christian C. Robert, editors, *Proceedings of the 19th International Conference on Artificial Intelligence and Statistics*, volume 51 of *Proceedings of Machine Learning Research*, pages 370–378, Cadiz, Spain, 09–11 May 2016. PMLR.
- [73] Andrew Gordon Wilson, Pavel Izmailov, Matthew D Hoffman, Yarin Gal, Yingzhen Li, Melanie F Pradier, Sharad Vikram, Andrew Foong, Sanae Lotfi, and Sebastian Farquhar. Evaluating approximate inference in bayesian deep learning. In Douwe Kiela, Marco Ciccone, and Barbara Caputo, editors, *Proceedings of the NeurIPS 2021 Competitions and Demonstrations Track*, volume 176 of *Proceedings of Machine Learning Research*, pages 113–124. PMLR, 2022.
- [74] Fei Zhu, Zhen Cheng, Xu-Yao Zhang, and Cheng-Lin Liu. Openmix: Exploring outlier samples for misclassification detection. In *Proceedings of the IEEE/CVF Conference on Computer Vision and Pattern Recognition*, pages 12074–12083, 2023.

A Appendix / supplemental material

A.1 Multi-Head Self-Attention

Self-Attention. Given an input of the attention layer $\mathbf{U} \in \mathbb{R}^{N \times d}$, where N is the number of data points and d is the embedding dimension, self-attention computes queries, keys, and values via $\mathbf{Q} = \mathbf{U}\mathbf{W}_q$, $\mathbf{K} = \mathbf{U}\mathbf{W}_k$, and $\mathbf{V} = \mathbf{U}\mathbf{W}_v$, with projection matrices $\mathbf{W}_q, \mathbf{W}_k, \mathbf{W}_v \in \mathbb{R}^{d \times d_h}$, where d_h is projected dimension. The output of the self-attention is:

$$\mathbf{F} = \text{softmax} \left(\frac{\mathbf{Q}\mathbf{K}^\top}{\sqrt{d_h}} \right) \mathbf{V} = \mathbf{A}_{qk} \mathbf{V}, \quad (13)$$

where attention matrix $\mathbf{A}_{qk} \in \mathbb{R}^{N \times N}$ encodes the pairwise similarity between the queries and keys.

Multi-Head Self-Attention (MHSA). MHSA employs n parallel attention heads, each independently computing a self-attention output $\mathbf{F}^{(h)}$ with corresponding $\mathbf{W}_q^{(h)}, \mathbf{W}_k^{(h)}, \mathbf{W}_v^{(h)} \in \mathbb{R}^{d \times d_h}$ as defined in Eq. 13. To maintain computational efficiency, the dimensionality of each head is typically set to $d_h = d/n$. The outputs from all attention heads are concatenated and subsequently projected back to the input dimension, forming MHSA's output:

$$\mathbf{R} = \mathbf{O} \left[\mathbf{F}^{(1)}, \mathbf{F}^{(2)}, \dots, \mathbf{F}^{(n)} \right] \quad (14)$$

where $\mathbf{O} \in \mathbb{R}^{d \times (n \cdot d_h)}$ is a projection matrix.

A.2 Self-Attention as Gaussian Process Inference

Kernel Attention or K-Attention [65] has extended the attention mechanism by replacing cosine similarity with a general kernel function $\kappa(\cdot, \cdot) : \mathbb{R}^d \times \mathbb{R}^d \rightarrow \mathbb{R}$ to compute pairwise similarities. Specifically, the attention matrix \mathbf{A}_{qk} is replaced by a kernel matrix \mathcal{K}_{qk} , where each entry is defined as $[\mathcal{K}_{qk}]_{i,j} = \kappa(\mathbf{U}_{i,:}, \mathbf{U}_{j,:})$. Consequently, the output of the kernel attention mechanism is:

$$\mathbf{F} = \mathcal{K}_{qk} \mathbf{V}, \quad (15)$$

Sparse Gaussian Process Attention (SGPA) [12] leverages the Sparse Variational Gaussian Process (SVGP) framework to approximate posterior variances in the attention mechanism. For each dimension i of attention output, the posterior mean and covariance are given by:

$$\mu_i = \mathcal{K}_{qk} \mathbf{V}_{:,i}, \text{ and } \Sigma_i = \mathcal{K}_{qq} + \mathcal{K}_{qk} \left(\mathcal{K}_{kk}^{-1} [\mathcal{S}]_{:,i} \mathcal{K}_{kk}^{-1} - \mathcal{K}_{kk}^{-1} \right) \mathcal{K}_{kq} \quad (16)$$

where $\mathcal{S} \in \mathbb{R}^{N \times N \times d_h}$ is a set of variational covariance parameters, optimized via the SVGP evidence lower bound. The output for each dimension i is then sampled using the reparameterization trick:

$$\mathbf{F}_{:,i} = \mu_i + \Sigma_i^{1/2} \cdot \epsilon_i, \quad \epsilon_i \sim \mathcal{N}(0, I) \quad (17)$$

By stacking the results across all d_h output dimensions, the final output of the attention head is:

$$\mathbf{F} = \left[\mu_1 + \Sigma_1^{1/2} \epsilon_1, \dots, \mu_{d_h} + \Sigma_{d_h}^{1/2} \epsilon_{d_h} \right] \in \mathbb{R}^{N \times d_h} \quad (18)$$

Kernel-Eigen Pair Sparse Variational Gaussian Processes Attention (KEP-SVGP) [15]. The constraint of imposing a symmetric kernel matrix \mathcal{K}_{qk} in **K-Attention** and **SGPA** (requiring $\mathbf{W}_q = \mathbf{W}_k$) can restrict the model's representation capacity by eliminating the inherent asymmetry of the original attention matrix \mathbf{A}_{qk} . To overcome this restriction, **KEP-SVGP** employs two Gaussian Processes (GPs), leveraging the symmetry of $\mathcal{K}_{qk} \mathcal{K}_{qk}^\top$ and $\mathcal{K}_{qk}^\top \mathcal{K}_{qk}$. Each attention output dimension is then computed by combining the contributions from the two GPs.

More specifically, building on the KSVD framework and the Primal-Attention formulation [13], KEP-SVGP introduces two sets of s -dimensional attention outputs to model the left and right eigenspaces, denoted as $F_{[i]}^e := F^e[:, i]$ and $F_{[i]}^r := F^r[:, i] \in \mathbb{R}^N$ for $i = 1, \dots, s$, corresponding to the primal features $e(\mathbf{U})$ and $r(\mathbf{U})$ in [13], respectively. To model these outputs, the following SVGP priors are defined based on the induced symmetric kernels $\mathcal{K}_{qk} \mathcal{K}_{qk}^\top$ and $\mathcal{K}_{qk}^\top \mathcal{K}_{qk}$:

$$\begin{pmatrix} \mathbf{F}_{[i]}^e \\ \mathbf{u}_i^e \end{pmatrix} \sim \mathcal{GP} \left(\mathbf{0}, \begin{pmatrix} \mathcal{K}_{qk} \mathcal{K}_{qk}^\top & \mathbf{H}_e \Lambda^2 \\ \Lambda^2 \mathbf{H}_e^\top & \Lambda^2 \end{pmatrix} \right), \quad \begin{pmatrix} \mathbf{F}_{[i]}^r \\ \mathbf{u}_i^r \end{pmatrix} \sim \mathcal{GP} \left(\mathbf{0}, \begin{pmatrix} \mathcal{K}_{qk}^\top \mathcal{K}_{qk} & \mathbf{H}_r \Lambda^2 \\ \Lambda^2 \mathbf{H}_r^\top & \Lambda^2 \end{pmatrix} \right), \quad (19)$$

where $\Lambda \in \mathbb{R}^{s \times s}$ is a diagonal matrix of the top- s singular values of \mathcal{K}_{qk} , and $\mathbf{H}_e, \mathbf{H}_r \in \mathbb{R}^{N \times s}$ contain the corresponding top- s left and right singular vectors, respectively. Using variational distributions $\mathbf{u}_{[i]}^e, \mathbf{u}_{[i]}^r \sim \mathcal{N}(\mathbf{m}_{\mathbf{u},[i]}, S_{\mathbf{u}\mathbf{u},[i]})$, closed-form posteriors $q(\mathbf{F}_i^c | \mathbf{U}) = \int q(\mathbf{F}_i^c | \mathbf{u}_i) q(\mathbf{u}_i) d\mathbf{u}_i$ ($c \in \{e, r\}$) are derived as:

$$\begin{aligned} q(\mathbf{F}_i^e | \mathbf{U}) &\sim \mathcal{N}\left(\underbrace{E_U \Lambda^{-1} \mathbf{m}_{\mathbf{u},[d]}}_{\mu^e := \mathbf{m}_{[i]}^e}, \underbrace{E_U \Lambda^{-2} S_{\mathbf{u}\mathbf{u},[i]} E_U^\top}_{\Sigma^e := \mathbf{L}_{[i]}^e \mathbf{L}_{[i]}^{e\top}}\right), \\ q(\mathbf{F}_i^r | \mathbf{U}) &\sim \mathcal{N}\left(\underbrace{R_U \Lambda^{-1} \mathbf{m}_{\mathbf{u},[d]}}_{\mu^r := \mathbf{m}_{[i]}^r}, \underbrace{R_U \Lambda^{-2} S_{\mathbf{u}\mathbf{u},[i]} R_U^\top}_{\Sigma^r := \mathbf{L}_{[i]}^r \mathbf{L}_{[i]}^{r\top}}\right), \end{aligned} \quad (20)$$

where $E_U := [e(\mathbf{U}_1), \dots, e(\mathbf{U}_N)]^\top \in \mathbb{R}^{N \times s}$ and $R_U := [r(\mathbf{U}_1), \dots, r(\mathbf{U}_N)]^\top \in \mathbb{R}^{N \times s}$ are the projection matrices w.r.t. right and left singular vectors of KSVD in [13]. The variational parameters are $\mathbf{m}_{\mathbf{u}} \in \mathbb{R}^{s \times s}$, $S_{\mathbf{u}\mathbf{u}} \in \mathbb{R}^{s \times s \times s}$ with the components i -th defined as $\mathbf{m}_{\mathbf{u},[i]} := \mathbf{m}_{\mathbf{u}}[:, i] \in \mathbb{R}^s$, and $S_{\mathbf{u}\mathbf{u},[i]} := S_{\mathbf{u}\mathbf{u}}[:, :, i] \in \mathbb{R}^{s \times s}$.

The outputs of the two SVGPs are sampled via the reparameterization trick:

$$F_{[i]}^e = \mathbf{m}_{[i]}^e + \mathbf{L}_{[i]}^e \epsilon, \quad F_{[i]}^r = \mathbf{m}_{[i]}^r + \mathbf{L}_{[i]}^r \epsilon, \quad \text{with } \epsilon \sim \mathcal{N}(0, I_N) \quad (21)$$

To fuse the outputs, two schemes are proposed: Addition ($F_{[i]}^{add} := F_{[i]}^e + F_{[i]}^r \in \mathbb{R}^N$) and Concatenation ($F_{[i]}^{cat} := [F_{[i]}^e; F_{[i]}^r] \in \mathbb{R}^{2N}$). To align with standard Transformer architecture, the s -dimensional attention outputs are linearly projected to the target dimension d_h . The final output $\mathbf{F} \in \mathbb{R}^{N \times d_h}$ is computed as: $\mathbf{F} = \mathbf{F}^{add} \mathbf{W}^{add}$ for the addition, $\mathbf{F} = \mathbf{W}_1^{cat} \mathbf{F}^{cat} \mathbf{W}_2^{cat}$ for the concatenation, where the projection matrices are $\mathbf{W}^{add} \in \mathbb{R}^{s \times d_h}$, $\mathbf{W}_1^{cat} \in \mathbb{R}^{N \times 2N}$ and $\mathbf{W}_2^{cat} \in \mathbb{R}^{s \times d_h}$.

A.3 Denoising Diffusion Probabilistic Models

Denoising Diffusion Probabilistic Models (DDPMs) [28] transform data into noise through a gradual forward diffusion process and then learn to reverse this transformation. The forward process incrementally adds Gaussian noise to the data \mathbf{X}_0 over T steps:

$$p(\mathbf{X}_t | \mathbf{X}_{t-1}) = \mathcal{N}(\mathbf{X}_t; \sqrt{1 - \beta_t} \mathbf{X}_{t-1}, \beta_t \mathbf{I}), \quad (22)$$

where $\{\beta_t\}_{t=1}^T$ controls the noise schedule. This defines a Markov chain that progressively corrupts the data. The true reverse process $p(\mathbf{X}_{t-1} | \mathbf{X}_t)$ is generally intractable but becomes tractable when conditioned on \mathbf{X}_0 :

$$p(\mathbf{X}_{t-1} | \mathbf{X}_t, \mathbf{X}_0) = \mathcal{N}(\mathbf{X}_{t-1}; \tilde{\mu}_t(\mathbf{X}_t, \mathbf{X}_0), \tilde{\beta}_t \mathbf{I}), \quad (23)$$

where closed-form expressions for $\tilde{\mu}_t$ and $\tilde{\beta}_t$ follow from Bayes' rule under the forward process. However, \mathbf{X}_0 is unknown at test time, the model instead learns a parameterized reverse process that conditions only on (\mathbf{X}_t, t) :

$$q_\theta(\mathbf{X}_{t-1} | \mathbf{X}_t) = \mathcal{N}(\mathbf{X}_{t-1}; \mu_\theta(\mathbf{X}_t, t), \Sigma_\theta(\mathbf{X}_t, t)), \quad (24)$$

Learning proceeds by minimizing the variational bound on the negative log-likelihood of the data, which encourages $q_\theta(\mathbf{X}_{t-1} | \mathbf{X}_t)$ to match the true reverse process $p(\mathbf{X}_{t-1} | \mathbf{X}_t, \mathbf{X}_0)$. This is typically implemented via noise prediction (score matching), where the network predicts the injected noise ϵ instead of μ_θ .

A.4 Derivation of the upper bound of $L(\theta)$

The negative log-likelihood $L(\theta) = \mathbb{E}_{p(\mathbf{X}_0 | \mathbf{X}_T)} [-\log q_\theta(\mathbf{X}_0 | \mathbf{X}_T)]$ is upper bounded by

$$L(\theta) \leq \mathbb{H}\left(p(\mathbf{X}_0 | \mathbf{X}_T)\right) + \sum_{t=1}^T \mathbb{E}_{p(\mathbf{X}_t | \mathbf{X}_T)} \left[D_{\text{KL}}\left(p(\mathbf{X}_{t-1} | \mathbf{X}_t) \parallel q_\theta(\mathbf{X}_{t-1} | \mathbf{X}_t)\right) \right] \quad (25)$$

Proof. From the definition of $L(\theta)$, we have

$$L(\theta) = -\mathbb{E}_{p(\mathbf{X}_0|\mathbf{X}_T)} [\log q_\theta(\mathbf{X}_0 | \mathbf{X}_T)] \quad (26)$$

$$= -\mathbb{E}_{p(\mathbf{X}_0|\mathbf{X}_T)} \left[\log \left(\int q_\theta(\mathbf{X}_{0:T-1} | \mathbf{X}_T) d\mathbf{X}_{1:T-1} \right) \right] \quad (27)$$

$$= -\mathbb{E}_{p(\mathbf{X}_0|\mathbf{X}_T)} \left[\log \left(\int p(\mathbf{X}_{1:T-1} | \mathbf{X}_0, \mathbf{X}_T) \frac{q_\theta(\mathbf{X}_{0:T-1} | \mathbf{X}_T)}{p(\mathbf{X}_{1:T-1} | \mathbf{X}_0, \mathbf{X}_T)} d\mathbf{X}_{1:T-1} \right) \right] \quad (28)$$

$$= -\mathbb{E}_{p(\mathbf{X}_0|\mathbf{X}_T)} \left[\log \left(\mathbb{E}_{p(\mathbf{X}_{1:T-1}|\mathbf{X}_0, \mathbf{X}_T)} \left[\frac{q_\theta(\mathbf{X}_{0:T-1} | \mathbf{X}_T)}{p(\mathbf{X}_{1:T-1} | \mathbf{X}_0, \mathbf{X}_T)} d\mathbf{X}_{1:T-1} \right] \right) \right] \quad (29)$$

$$\leq -\mathbb{E}_{p(\mathbf{X}_{0:T-1}|\mathbf{X}_T)} \log \left(\frac{q_\theta(\mathbf{X}_{0:T-1} | \mathbf{X}_T)}{p(\mathbf{X}_{1:T-1} | \mathbf{X}_0, \mathbf{X}_T)} \right) \quad (\text{Jensen's inequality}) \quad (30)$$

$$= \mathbb{E}_{p(\mathbf{X}_{0:T-1}|\mathbf{X}_T)} \log \left(\frac{p(\mathbf{X}_{1:T-1} | \mathbf{X}_0, \mathbf{X}_T)}{q_\theta(\mathbf{X}_{0:T-1} | \mathbf{X}_T)} \right) = L_{VLB} \quad (31)$$

Now, we derive the L_{VLB} as follows:

$$L_{VLB} = \mathbb{E}_{p(\mathbf{X}_{0:T-1}|\mathbf{X}_T)} \left[\log \left(\frac{p(\mathbf{X}_{1:T-1} | \mathbf{X}_0, \mathbf{X}_T)}{q_\theta(\mathbf{X}_{0:T-1} | \mathbf{X}_T)} \right) \right] \quad (32)$$

$$= \mathbb{E}_{p(\mathbf{X}_{0:T-1}|\mathbf{X}_T)} \left[\log \left(\frac{p(\mathbf{X}_{0:T-1} | \mathbf{X}_T)}{q_\theta(\mathbf{X}_{0:T-1} | \mathbf{X}_T) p(\mathbf{X}_0 | \mathbf{X}_T)} \right) \right] \quad (33)$$

$$= \mathbb{E}_{p(\mathbf{X}_{0:T-1}|\mathbf{X}_T)} \left[-\log p(\mathbf{X}_0 | \mathbf{X}_T) + \log \left(\frac{p(\mathbf{X}_{0:T-1} | \mathbf{X}_T)}{q_\theta(\mathbf{X}_{0:T-1} | \mathbf{X}_T)} \right) \right] \quad (34)$$

$$= \mathbb{E}_{p(\mathbf{X}_{0:T-1}|\mathbf{X}_T)} \left[-\log p(\mathbf{X}_0 | \mathbf{X}_T) + \log \left(\prod_{t=1}^T \frac{p(\mathbf{X}_{t-1} | \mathbf{X}_t)}{q_\theta(\mathbf{X}_{t-1} | \mathbf{X}_t)} \right) \right] \quad (35)$$

$$= \mathbb{E}_{p(\mathbf{X}_{0:T-1}|\mathbf{X}_T)} \left[-\log p(\mathbf{X}_0 | \mathbf{X}_T) + \sum_{t=1}^T \log \left(\frac{p(\mathbf{X}_{t-1} | \mathbf{X}_t)}{q_\theta(\mathbf{X}_{t-1} | \mathbf{X}_t)} \right) \right] \quad (36)$$

$$= \mathbb{H}(p(\mathbf{X}_0 | \mathbf{X}_T)) + \sum_{t=1}^T \mathbb{E}_{p(\mathbf{X}_{0:T-1}|\mathbf{X}_T)} \left[\log \left(\frac{p(\mathbf{X}_{t-1} | \mathbf{X}_t)}{q_\theta(\mathbf{X}_{t-1} | \mathbf{X}_t)} \right) \right] \quad (37)$$

Additionally, we have:

$$\mathbb{E}_{p(\mathbf{X}_{0:T-1}|\mathbf{X}_T)} \left[\log \left(\frac{p(\mathbf{X}_{t-1} | \mathbf{X}_t)}{q_\theta(\mathbf{X}_{t-1} | \mathbf{X}_t)} \right) \right] \quad (38)$$

$$= \int p(\mathbf{X}_{0:T-1} | \mathbf{X}_T) \log \left(\frac{p(\mathbf{X}_{t-1} | \mathbf{X}_t)}{q_\theta(\mathbf{X}_{t-1} | \mathbf{X}_t)} \right) d\mathbf{X}_{0:T-1} \quad (39)$$

$$= \int p(\mathbf{X}_{t-1}, \mathbf{X}_t | \mathbf{X}_T) \log \left(\frac{p(\mathbf{X}_{t-1} | \mathbf{X}_t)}{q_\theta(\mathbf{X}_{t-1} | \mathbf{X}_t)} \right) d\mathbf{X}_{t-1} d\mathbf{X}_t \quad (40)$$

$$= \int p(\mathbf{X}_t | \mathbf{X}_T) p(\mathbf{X}_{t-1} | \mathbf{X}_t) \log \left(\frac{p(\mathbf{X}_{t-1} | \mathbf{X}_t)}{q_\theta(\mathbf{X}_{t-1} | \mathbf{X}_t)} \right) d\mathbf{X}_{t-1} d\mathbf{X}_t \quad (41)$$

$$= \mathbb{E}_{p(\mathbf{X}_t|\mathbf{X}_T)} \left[D_{KL} \left(p(\mathbf{X}_{t-1} | \mathbf{X}_t) \parallel q_\theta(\mathbf{X}_{t-1} | \mathbf{X}_t) \right) \right] \quad (42)$$

A.5 Practical implementation of the proposed algorithm in Eq.12

The uncertainty-aware transition parameterization can be obtained via the objective in Eq.12:

$$\theta = \arg \min_{\theta} \left\{ L_1(\theta) + L_2(\theta) \right\} \quad (43)$$

which combines the matching loss

$$L_1(\theta) = \mathbb{E}_{(\mathbf{X}_t, t) \sim p(\mathbf{X}_t|\mathbf{X}_T)} \left[D_{KL} \left(p(\mathbf{X}_{t-1} | \mathbf{X}_t) \parallel q_\theta(\mathbf{X}_{t-1} | \mathbf{X}_t) \right) \right], \quad (44)$$

with the performance-aware loss

$$L_2(\theta) = \mathbb{E}_{(\mathbf{X}, \mathbf{y}) \sim \mathcal{D}} \mathbb{E}_{\mathbf{X}_0 \sim q_\theta(\mathbf{X}_0 | \mathbf{X}_T)} \left[\text{loss}(\mathbf{X}_0, \mathbf{y}) \right], \quad (45)$$

where \mathbf{X} is sampled from the training dataset \mathcal{D} and is embedded with $\mathbf{X}_T = \text{embed}(\mathbf{X})$. \mathbf{X}_0 is then sampled via iteratively simulating the current estimate of the probability path $q_\theta(\mathbf{X}_{t-1} | \mathbf{X}_t)$. In addition, the KL divergence in Eq. 44 can be reduced to the following loss,

$$D_{\text{KL}}(p \parallel q_\theta) \propto \frac{1}{2} \left[\text{tr} [\sigma_\theta(\mathbf{X}_t, t)^{-1} \sigma_t(\mathbf{X}_t)] + \log \frac{|\sigma_\theta(\mathbf{X}_t, t)|}{|\sigma_t(\mathbf{X}_t)|} \right] \quad (46)$$

$$+ \frac{1}{2} \left(m_\theta(\mathbf{X}_t, t) - m_t(\mathbf{X}_t) \right)^\top \sigma_\theta(\mathbf{X}_t)^{-1} \left(m_\theta(\mathbf{X}_t, t) - m_t(\mathbf{X}_t) \right). \quad (47)$$

However, the KL computation still presents a challenge due to the high dimensionality of the covariance matrix $\sigma_t(\mathbf{X}_t)$, which complicates the evaluation of the trace and log-determinant terms. To mitigate this, we follow the approach of KEP by approximating $\sigma_t(\mathbf{X}_t)$ using a Cholesky-like factor \mathbf{L}_t such that $\sigma_t(\mathbf{X}_t) = \mathbf{L}_t \mathbf{L}_t^\top$. For the learned covariance $\sigma_\theta(\mathbf{X}_t, t)$, we employ a diagonal parameterization, whose Cholesky-like factor reduces to the element-wise square root of its diagonal entries. As demonstrated in Appendix A.6.5, this choice is substantially more efficient than a full covariance parameterization without sacrificing performance. Matching these Cholesky-like factors ensures that the corresponding covariance matrices are aligned, effectively nullifying the trace and log-determinant terms in the KL divergence and enabling efficient optimization. Employing Cholesky-like factor and incorporating weighting terms yields the final objective:

$$\theta = \arg \min_{\theta} \left\{ \lambda_{\text{mean}} L_{\text{mean}}(\theta) + \lambda_{\text{Cholesky}} L_{\text{Cholesky}}(\theta) + \lambda_{\text{NLL}} L_2(\theta) \right\}, \quad (48)$$

where λ_{mean} , $\lambda_{\text{Cholesky}}$, and λ_{NLL} are weighting coefficients for the mean matching term, the Cholesky-like factor alignment, and the performance-aware loss, respectively. The individual loss components are defined as follows:

$$L_{\text{mean}}(\theta) = \frac{1}{T} \sum_{t=1}^T \mathbb{E}_{p(\mathbf{X}_t | \mathbf{X}_T)} \left[\|m_\theta(\mathbf{X}_t, t) - m_t(\mathbf{X}_t)\|_2^2 \right], \quad (49)$$

$$L_{\text{Cholesky}}(\theta) = \frac{1}{T} \sum_{t=1}^T \mathbb{E}_{p(\mathbf{X}_t | \mathbf{X}_T)} \left[\left\| \left(\sigma_\theta(\mathbf{X}_t, t)^{1/2} - \text{Chol}(\sigma_t(\mathbf{X}_t)) \right) \right\|_2^2 \right], \quad (50)$$

$$L_2(\theta) = \mathbb{E}_{(\mathbf{X}, \mathbf{y}) \sim \mathcal{D}} \mathbb{E}_{\mathbf{X}_0 \sim q_\theta(\mathbf{X}_0 | \mathbf{X}_T)} \left[\text{loss}(\mathbf{X}_0, \mathbf{y}) \right], \quad (51)$$

where $\text{Chol}(\cdot)$ denotes the Cholesky-like factorization. We provide the pseudocode for one training iteration of DIRECTOR in Algorithm 1.

Algorithm 1 One training iteration of DIRECTOR. The pre-trained backbone f is frozen.

Input: training pair (\mathbf{X}, \mathbf{y}) ; pre-trained backbone f with T reconfigured blocks; transition model q_θ with parameters θ ; loss weights $\lambda_{\text{mean}}, \lambda_{\text{Cholesky}}, \lambda_{\text{NLL}}$; learning rate η .

Output: updated transition-model parameters θ .

- 1: Embed input: $\mathbf{X}_T \leftarrow \text{embed}(\mathbf{X})$. {shared with the backbone}
 - 2: With f frozen, run a forward pass to obtain the trajectory $\{\mathbf{X}_t\}_{t=0}^T$ and, at each block, the ground-truth Gaussian transition statistics $\{(m_t(\mathbf{X}_t), \sigma_t(\mathbf{X}_t))\}_{t=1}^T$ (Eq. 5).
 - 3: **for** $t = 1, \dots, T$ **do**
 - 4: Predict $(m_\theta(\mathbf{X}_t, t), \sigma_\theta(\mathbf{X}_t, t)) \leftarrow q_\theta(\mathbf{X}_t, t)$. {single-block DiT}
 - 5: **end for**
 - 6: Roll out $\mathbf{X}_0 \sim q_\theta(\mathbf{X}_0 | \mathbf{X}_T)$ and pass through the classification head to obtain logits $\hat{\mathbf{y}}$.
 - 7: $L_{\text{mean}} \leftarrow \frac{1}{T} \sum_{t=1}^T \|m_\theta(\mathbf{X}_t, t) - m_t(\mathbf{X}_t)\|_2^2$ {Eq. 49}
 - 8: $L_{\text{Cholesky}} \leftarrow \frac{1}{T} \sum_{t=1}^T \|\sigma_\theta(\mathbf{X}_t, t)^{1/2} - \text{Chol}(\sigma_t(\mathbf{X}_t))\|_2^2$ {Eq. 50}
 - 9: $L_{\text{NLL}} \leftarrow \text{CE}(\hat{\mathbf{y}}, \mathbf{y})$ {Eq. 51}
 - 10: $\mathcal{L}(\theta) \leftarrow \lambda_{\text{mean}} L_{\text{mean}} + \lambda_{\text{Cholesky}} L_{\text{Cholesky}} + \lambda_{\text{NLL}} L_{\text{NLL}}$ {Eq. 12}
 - 11: $\theta \leftarrow \theta - \eta \nabla_{\theta} \mathcal{L}(\theta)$
 - 12: **return** θ
-

A.6 Additional experiments

A.6.1 Large-scale experiment

Table 6: Comparison of average performance achieved a pre-trained ViT-B-16 model (fine-tuned on CIFAR-10) and its reconfigured variant produced by DIRECTOR.

Method	#params	ACC \uparrow	ECE \downarrow	NLL \downarrow	Brier \downarrow
ViT-B-16	86M	97.880	18.021	2.564	6.843
DIRECTOR	50M	97.170	1.611	1.122	4.762

Table 7: Comparison of average performance achieved a pre-trained Qwen-2.5 model (fine-tuned on SST-2) and its reconfigured variant produced by DIRECTOR.

Method	#params	ACC \uparrow	ECE \downarrow	NLL \downarrow	Brier \downarrow
Qwen-2.5	0.494B	93.005	5.864	3.300	12.184
DIRECTOR	0.479B	93.119	5.482	2.953	12.089

To stress test DIRECTOR, we further evaluate its scalability on a larger-scale experiment which requires reconfiguring a pre-trained ViT-B-16 model (pre-trained on the large-scale ImageNet data and fine-tuned on CIFAR-10 data). The reported results in Table 6 show that DIRECTOR’s reconfigured ViT-B-16 achieves substantially better uncertainty calibration with an ECE of 1.611 compared to 18.021 of the original ViT-B-16. DIRECTOR also maintains competitive predictive performance (97.17% vs. 97.88%) while requiring significantly fewer parameters (50M vs. 86M). These findings highlight the ability of DIRECTOR to deliver reliable uncertainty calibration even in large and complex transformer architectures, pre-trained on sophisticated and large-scale data.

We further evaluate the scalability of DIRECTOR to a large-scale pre-trained language model by reconfiguring the last three transformer blocks of a Qwen-2.5 model fine-tuned on SST-2; due to the compute cost of a full-stack reconfiguration on a billion-parameter language model, the remaining blocks retain their original deterministic computation. The reported results in Table 7 show that DIRECTOR’s reconfigured Qwen-2.5 achieves better uncertainty calibration with an ECE of 5.482 compared to 5.864 of the original Qwen-2.5, together with consistent improvements across the other calibration metrics, reducing NLL from 3.300 to 2.953 and Brier from 12.184 to 12.089. DIRECTOR also slightly improves predictive accuracy (93.119% vs. 93.005%) while requiring fewer parameters (0.479B vs. 0.494B). These findings highlight the ability of DIRECTOR to deliver reliable uncertainty calibration even in large pre-trained language models.

A.6.2 Deep Ensembles Results

We further evaluate the performance of Deep Ensembles [33], a simple yet effective method for uncertainty estimation, when combined with pretrained models and DIRECTOR, as reported in Table 8. The results show that DIRECTOR consistently outperforms pretrained models across both CIFAR-10 and IMDB. On CIFAR-10, DIRECTOR achieves notable improvements in predictive accuracy (up to +5.8% over KEP-7/7), while also delivering stronger uncertainty calibration (lower ECE and NLL) and robustness (AURC, AUROC, Brier score). On IMDB, although the baseline Transformer ensemble already achieves strong results, DIRECTOR further improves calibration (ECE, NLL, Brier) and robustness metrics, with the exception of AURC and AUROC where the Transformer baseline performs slightly better. Overall, these findings demonstrate that DIRECTOR works effectively to ensemble settings, providing consistent benefits across architectures, datasets, and evaluation metrics.

A.6.3 Reconfiguring the SGPA Backbone

As discussed in Section 3.2, SGPA exhibits a pronounced trade-off between calibration and predictive performance, achieving low ECE on CIFAR-10 (1.92) at the cost of a substantially lower accuracy

Table 8: Performance comparison of Deep Ensembles for in-distribution classification on CIFAR-10 and IMDB. KEP- k/n denotes a pre-trained transformer using GP-reparameterized architecture (KEP [15]) for the last k attention blocks and standard MHSA for the remaining blocks. **Bold** indicates the better performance in each pairwise comparison between a baseline ensemble (ViT, Transformer, KEP) and diffusion-based reconfigured KEP [15] produced by DIRECTOR ensemble.

Dataset	Method	ACC \uparrow	AURC \downarrow	AUROC \uparrow	FPR95 \downarrow	ECE \downarrow	NLL \downarrow	Brier \downarrow
CIFAR-10	ViT	87.21	2.52	88.84	58.41	2.70	5.14	19.01
	DIRECTOR	88.82	1.91	90.09	52.77	1.72	3.69	16.38
	KEP-1/7	87.48	2.33	89.43	56.39	2.30	4.46	18.29
	DIRECTOR	89.32	1.78	90.12	54.31	1.67	3.50	15.76
	KEP-2/7	87.09	2.41	89.48	54.07	2.71	4.48	18.69
	DIRECTOR	89.20	1.79	90.33	51.85	1.86	3.52	15.73
IMDB	Transformer	87.31	3.55	82.92	71.45	2.36	3.04	18.44
	DIRECTOR	87.45	3.56	82.83	70.68	1.97	3.00	18.25
	KEP-1/5	87.44	3.63	82.34	72.21	1.56	3.01	18.39
	DIRECTOR	87.85	3.44	83.20	71.10	1.25	2.89	17.62
	KEP-2/5	87.77	3.51	82.44	73.14	2.85	3.04	18.18
	DIRECTOR	87.88	3.43	82.96	72.29	1.24	2.91	17.70
IMDB	KEP-5/5	86.49	4.16	81.54	74.07	2.63	3.28	19.72
	DIRECTOR	87.66	3.43	82.95	72.13	2.07	2.95	18.05

Table 9: Reconfiguring an SGPA backbone with DIRECTOR across CIFAR-10, IMDB, and CoLA. SGPA rows reproduce the values reported in Table 2. **Bold** indicates the better value within each pairwise comparison.

Dataset	Method	ACC/MCC \uparrow	AURC \downarrow	AUROC \uparrow	FPR95 \downarrow	ECE \downarrow	NLL \downarrow	Brier \downarrow
CIFAR-10	SGPA	75.59 \pm 3.63	8.41 \pm 2.37	82.65 \pm 1.71	71.78 \pm 2.73	1.92 \pm 0.55	7.11 \pm 0.95	33.98 \pm 4.57
	DIRECTOR	82.65 \pm 1.16	4.47 \pm 0.56	86.00 \pm 0.65	66.39 \pm 2.34	4.53 \pm 0.58	5.30 \pm 0.29	25.10 \pm 1.48
IMDB	SGPA	85.39 \pm 0.36	4.96 \pm 0.49	80.04 \pm 1.14	76.44 \pm 0.96	6.04 \pm 1.71	3.96 \pm 0.50	22.19 \pm 1.06
	DIRECTOR	86.16 \pm 0.62	4.44 \pm 0.44	81.04 \pm 0.76	74.67 \pm 1.43	3.12 \pm 1.43	3.36 \pm 0.16	20.30 \pm 0.84
CoLA	SGPA	31.53 \pm 2.05	20.44 \pm 2.60	64.34 \pm 1.95	90.79 \pm 0.87	26.22 \pm 1.51	28.65 \pm 7.23	54.08 \pm 2.44
	DIRECTOR	32.84 \pm 2.66	19.04 \pm 1.26	64.67 \pm 1.18	89.38 \pm 1.46	17.00 \pm 7.62	13.43 \pm 6.22	45.72 \pm 5.09

(75.59%) compared to its ViT and KEP counterparts. A natural question is whether DIRECTOR can mitigate this trade-off by reconfiguring an SGPA backbone in the same way it reconfigures KEP-SVGP and ViT. To this end, we apply our diffusion-based reconfiguration on top of a pre-trained SGPA backbone [12], following the same two-stage protocol used throughout the paper: we first train an SGPA backbone on each dataset and then train a single-block DiT-based transition model on top of the frozen SGPA features, using the same loss-weighting search procedure described in Appendix A.6.12. The resulting performance, alongside the SGPA stage-1 baseline reported in Table 2, is summarized in Table 9.

As shown in Table 9, DIRECTOR achieves higher predictive performance than the SGPA backbone across all three datasets, with a particularly large gain on CIFAR-10 (82.65% versus 75.59% in ACC) and consistent gains on IMDB (86.16% versus 85.39% in ACC) and CoLA (32.84 versus 31.53 in MCC). On CIFAR-10, DIRECTOR improves two of the three calibration metrics (NLL from 7.11 to 5.30, Brier from 33.98 to 25.10) and all three failure-prediction metrics (AURC from 8.41 to 4.47, AUROC from 82.65 to 86.00, FPR95 from 71.78 to 66.39), with ECE being the only column where SGPA retains a smaller value (1.92 versus 4.53). Although SGPA achieves the lowest CIFAR-10 ECE, this result reflects an unfavorable accuracy/calibration trade-off rather than genuinely well-calibrated predictions: ECE alone does not measure predictive utility, and on a balanced 10-class dataset such as CIFAR-10 a random guesser that always outputs the uniform distribution is perfectly calibrated in expectation, with confidence 0.1 matching accuracy 0.1. Reading ECE jointly with NLL and Brier,

Table 10: In-distribution calibration on CIFAR-10 after applying post-hoc Temperature Scaling (TS) to every baseline. **Bold** marks the better value within each pairwise comparison; **blue** marks the best value across the whole table.

Method	ACC \uparrow	AURC \downarrow	AUROC \uparrow	FPR95 \downarrow	ECE \downarrow	NLL \downarrow	Brier \downarrow
ViT + TS	83.84 \pm 0.09	3.88 \pm 0.09	86.82 \pm 0.33	65.99 \pm 1.73	9.20 \pm 0.32	6.57 \pm 0.14	25.49 \pm 0.12
DIRECTOR + TS	85.67 \pm 0.88	3.04 \pm 0.40	88.27 \pm 0.83	60.65 \pm 1.23	5.68 \pm 0.51	4.76 \pm 0.30	21.45 \pm 1.22
KEP-1/7 + TS	84.52 \pm 0.25	3.43 \pm 0.10	87.85 \pm 0.23	63.22 \pm 0.95	6.97 \pm 0.19	5.36 \pm 0.08	23.32 \pm 0.29
DIRECTOR + TS	86.51 \pm 0.57	2.73 \pm 0.15	88.65 \pm 0.22	59.89 \pm 0.61	4.64 \pm 0.26	4.33 \pm 0.15	20.01 \pm 0.62

which jointly penalize under-confident predictions and predictive errors, shows that DIRECTOR delivers a substantially better calibration profile overall (NLL 5.30 versus 7.11 and Brier 25.10 versus 33.98) while raising ACC from 75.59% to 82.65%. On IMDB and CoLA, DIRECTOR additionally reduces ECE, NLL, and Brier simultaneously, mirroring the trend observed for the KEP backbone in Table 1. These results demonstrate that the proposed reconfiguration extends naturally to the SGPA backbone, closing the predictive-performance gap that SGPA exhibits in Table 2 while retaining the calibration trade-off pattern observed for ViT and KEP in Section 3.

A.6.4 Effect of Post-hoc Temperature Scaling on Every Baseline

To examine whether the calibration gains reported by DIRECTOR can be explained by a single temperature parameter, we apply post-hoc TS to *every* baseline considered in the in-distribution setting on CIFAR-10, including the GP-aware variants (KEP- k/n and SGPA) that are typically left untouched in the literature. For each baseline, a single temperature scalar is fitted by minimizing the validation NLL via L-BFGS and is then applied to the test-time logits. The resulting in-distribution metrics, averaged over five random seeds and computed on the same checkpoints used to produce Table 1, are summarized in Table 10.

As shown in Table 10, DIRECTOR outperforms each TS-calibrated baseline pairwise on every metric. Within the ViT pair, DIRECTOR + TS improves ACC from 83.84% to 85.67% and ECE from 9.20 to 5.68, while also reducing AURC, NLL, and Brier scores. The same pattern holds within the KEP-1/7 pair, where every metric improves under DIRECTOR, and DIRECTOR (from KEP-1/7) + TS achieves the best value across the whole table on ACC, AURC, AUROC, FPR95, ECE, NLL, and Brier. These results confirm that the improvements reported in Section 3 originate from the diffusion-based reconfiguration itself, and not from the absence of post-hoc calibration on the baselines, and that the calibration improvements offered by DIRECTOR cannot be replicated by simply applying post-hoc TS to existing uncertainty-aware transformers.

A.6.5 Varying covariance structures

The covariance of the pretrained feature distribution, denoted by $\sigma_t(X_t)$, is approximated using a Cholesky-like factorization as employed in KEP-SVGP [15], which we select as the pretrained model for consistency. In addition, we adopt a diagonal parameterization for the learned covariance $\sigma_\theta(X_t, t)$, a design choice that is standard in diffusion models [28].

To examine whether this simplification compromises calibration quality, we conduct a small-scale empirical study comparing the diagonal parameterization against another alternative covariance structure, full parameterization. The results, summarized in Table 11, demonstrate that the diagonal approximation not only yields significantly faster training time but also achieves superior calibration performance relative to the more expressive covariance structure. These observations support the efficiency and effectiveness of the diagonal covariance design in our probabilistic reconfiguration framework.

We additionally report the wall-clock training time of the pretrained baselines, which corresponds to the cost of pre-training the underlying ViT or KEP-1/7 backbone for 300 epochs on CIFAR-10. As shown in the last column of Table 11, the ViT and KEP-1/7 backbones require roughly 3.85 and 6.51 hours respectively, while the unified transition model with the diagonal covariance parameterization is trained on top of either backbone in only 1.75 hours. The diffusion-based reconfiguration step

Table 11: Comparison of different covariance structures under two pretrained baselines ViT and KEP-1/7.

Baseline	Covariance Structure	ACC \uparrow	AURC \downarrow	AUROC \uparrow	FPR95 \downarrow	ECE \downarrow	NLL \downarrow	Brier \downarrow	Training time (hours)
ViT	Diagonal	86.38	2.70	88.80	61.16	9.00	6.34	22.21	1.75
	Full (dimension-wise)	81.55	4.95	85.48	68.08	10.70	7.28	28.88	2.50
	Baseline	83.90	4.02	86.71	65.16	12.57	10.94	27.80	3.85
KEP-1/7	Diagonal	86.22	2.83	88.35	61.90	8.85	6.21	22.23	1.75
	Full (dimension-wise)	83.80	3.81	87.26	62.10	11.16	8.12	26.34	2.50
	Baseline	84.61	3.52	87.44	65.04	10.86	8.17	25.59	6.51

Table 12: Inference time and memory consumption on CIFAR-10.

Method	Inference Time (s)	Inference Memory (GB)
KEP-7/7	2.1038	0.3348
KEP-1/7	1.5129	0.2916
SGPA	4.5169	0.5768
ViT	1.3173	0.1509
DIRECTOR	1.6756	0.1040

in DIRECTOR is therefore substantially less expensive than the original pretraining stage, supporting its use as a lightweight post-hoc add-on to existing pretrained transformers.

A.6.6 Computational and memory overhead

We evaluate the computational and memory overhead of our method against several baselines on the CIFAR-10 dataset. As reported in Table 12, our approach achieves substantially lower inference memory consumption than all competing methods, while maintaining an inference time comparable to KEP-1/7.

A.6.7 Varying unified transition models

Regarding kernel design, although score networks in diffusion models are commonly implemented using multilayer perceptrons (MLPs), our empirical results indicate that a DiT-based architecture [45] consistently achieves superior performance. Table 13 reports a comparison between MLP and DiT-based score networks on the CIFAR-10 dataset under two different pretrained baselines. While MLP-based score networks exhibit slightly better calibration on certain metrics, they underperform the corresponding baselines on most other evaluation criteria, particularly predictive accuracy. In contrast, the DiT-based architecture improves performance across the majority of metrics without sacrificing stability. Consequently, we adopt DiT as the score network in our framework.

A.6.8 Statistical significance testing

Regarding statistical significance, we report hypothesis testing results for both the CV task (CIFAR-10) and the NLP task (CoLA), corresponding to the results in Table 1. For CoLA, we additionally perform an extensive evaluation with 40 runs and compute paired t-tests across metrics.

As summarized in Table 14, the majority of comparisons yield p -values below 0.05, indicating that the observed improvements of our method over the corresponding baselines are statistically significant. This holds consistently across accuracy, uncertainty-aware metrics, and calibration measures, demonstrating the robustness of our performance gains.

A.6.9 Comparison with Knowledge Distillation

We compare DIRECTOR with knowledge distillation (KD) [27]. Results are presented in Table 15. We evaluate KD using a pretrained 7-layer ViT as the teacher and a 3-layer ViT or our DiT as the student, trained with KD (temperature scaling = 3), while DIRECTOR use DiT and trained with our loss function. Although KD improves accuracy, its calibration metrics remain higher compared to DIRECTOR, which achieves superior accuracy and calibration. Additionally, our propagation

Table 13: Comparison of unified transition model (UTM) architectures on CIFAR-10 under different pretrained baselines.

Baseline	UTM	ACC \uparrow	AURC \downarrow	AUROC \uparrow	FPR95 \downarrow	ECE \downarrow	NLL \downarrow	Brier \downarrow
ViT	MLP	81.17	5.11	85.47	67.39	1.36	5.52	26.70
	DiT	86.18	2.95	87.74	63.82	8.90	6.27	22.62
	Baseline	83.90	4.02	86.71	65.16	12.57	10.94	27.80
KEP-7/7	MLP	83.46	4.16	85.95	65.18	4.99	5.34	24.37
	DiT	87.37	2.43	88.99	60.97	8.53	6.07	20.84
	Baseline	82.34	4.42	86.45	65.80	5.81	5.59	25.68

Table 14: Significance testing results on CIFAR-10 (DF=4) and CoLA (DF=39). We report mean \pm standard error of performance (Perf.) and paired p -values.

Dataset	Method	ACC/MCC \uparrow		AURC \downarrow		AUROC \uparrow		FPR95 \downarrow		ECE \downarrow		NLL \downarrow		Brier \downarrow	
		Perf.	p	Perf.	p	Perf.	p	Perf.	p	Perf.	p	Perf.	p	Perf.	p
CIFAR-10	ViT	83.84 \pm 0.09	-	4.05 \pm 0.11	-	86.42 \pm 0.37	-	67.13 \pm 1.98	-	12.51 \pm 0.20	-	10.91 \pm 0.39	-	28.03 \pm 0.15	-
	DIRECTOR	85.67\pm0.88	0.0094	3.10\pm0.45	0.0054	87.90\pm1.04	0.0255	61.92\pm1.85	0.0104	9.67\pm0.62	0.0008	6.94\pm0.52	0.0001	23.54\pm1.46	0.0020
	KEP-1/7	84.52 \pm 0.25	-	3.52 \pm 0.11	-	87.52 \pm 0.27	-	65.14 \pm 1.27	-	10.93 \pm 0.26	-	8.21 \pm 0.15	-	25.80 \pm 0.40	-
	DIRECTOR	86.51\pm0.57	0.0051	2.78\pm0.16	0.0034	88.28\pm0.16	0.0065	61.85\pm1.93	0.0149	8.61\pm0.49	0.0020	6.11\pm0.27	0.0003	21.90\pm0.82	0.0020
	KEP-7/7	82.68 \pm 0.12	-	4.46 \pm 0.05	-	85.71 \pm 0.34	-	66.90 \pm 1.78	-	6.95 \pm 0.36	-	5.89 \pm 0.11	-	25.90 \pm 0.23	-
	DIRECTOR	84.74\pm0.40	0.0000	3.47\pm0.18	0.0000	87.34\pm0.33	0.0001	62.88\pm1.20	0.0023	5.18\pm0.33	0.0000	4.84\pm0.11	0.0000	22.48\pm0.53	0.0006
CoLA	Transformer	29.92 \pm 1.06	-	20.80 \pm 1.09	-	64.22 \pm 1.33	-	90.01 \pm 2.58	-	26.44 \pm 1.72	-	19.66 \pm 3.79	-	55.09 \pm 2.43	-
	DIRECTOR	31.97\pm2.26	0.0000	19.87\pm1.46	0.0004	64.52\pm1.44	-	89.94\pm2.02	0.8877	23.33\pm4.51	0.0001	15.30\pm5.62	0.0001	51.04\pm4.80	0.0000
	KEP-1/5	32.40 \pm 2.32	-	19.94 \pm 1.66	-	64.42 \pm 2.36	-	90.21 \pm 2.12	-	22.45 \pm 4.94	-	15.24 \pm 5.89	-	50.27 \pm 4.65	-
	DIRECTOR	31.41\pm2.05	0.0429	18.91\pm1.90	0.0098	65.45\pm1.72	0.0269	89.58\pm1.61	0.1484	17.47\pm8.87	0.0027	11.87\pm5.96	0.0128	46.62\pm6.91	0.0069
	KEP-5/5	31.36 \pm 2.73	-	19.80 \pm 1.92	-	64.66 \pm 0.98	-	90.26 \pm 1.15	-	19.87 \pm 5.69	-	14.74 \pm 8.28	-	48.69 \pm 5.57	-
	DIRECTOR	31.53\pm1.95	0.7545	18.58\pm2.49	0.0121	65.33\pm1.93	0.0361	88.70\pm1.63	0.0000	15.74\pm8.57	0.0139	10.80\pm5.91	0.0174	44.76\pm6.98	0.0076

model is highly parameter-efficient, using only 2.7M parameters, less than half of the original model’s 6.27M parameters, resulting in improved memory efficiency.

A.6.10 In-Distribution Classification

We consolidate the experimental results from Table 1 and Table 2, and further include additional findings based on our alignment with KEP-2/7 (vision) and KEP-2/5 (language) configurations, presented in Table 16. DIRECTOR demonstrates state-of-the-art performance across nearly all scenarios, achieving the **highest** score in 23 out of 28 settings and ranking **second** in another 23 out of 28. These results highlight the substantial advantage of DIRECTOR over existing baselines, in terms of both predictive accuracy and uncertainty calibration.

A.6.11 Distribution shift robustness

Additional experiments evaluating the distributional robustness of DIRECTOR are presented in Tables 17, 18, and Figure 3. These results include evaluations of DIRECTOR aligned with KEP-2/5 and KEP-2/7 configurations. Notably, the TS baseline is excluded from these comparisons, as it is specifically tailored for in-distribution tasks.

Figure 3 illustrates a calibration comparison between pre-trained models (ViT, KEP) and DIRECTOR on the CIFAR-10-C dataset, across five corruption severity levels averaged over 15 corruption types. DIRECTOR demonstrates competitive, and in many cases superior, predictive accuracy, particularly when aligned with KEP-7/7. In terms of uncertainty calibration, DIRECTOR exhibits significantly improved calibration, achieving lower values in ECE, NLL, and Brier score compared to pre-trained baselines.

Table 17 summarizes performance averaged over the 15 corruptions and five severity levels on CIFAR-10-C. While maintaining competitive predictive accuracy with ViT and KEP, DIRECTOR substantially outperforms them in calibration metrics. When aligned with KEP-2/7, our best-performing configuration of DIRECTOR achieves both competitive accuracy and slightly improved calibration compared to other baselines. Additionally, DIRECTOR can be enhanced by integrating post-training baselines such as MCD or aligning with attention-modified methods like SGPA to further improve calibration. However, due to computational constraints, we leave these extensions for future investigation.

Table 15: Performance comparison between knowledge distillation methods and our method on CIFAR-10 and CIFAR-100. Mean \pm std are reported over five trials.

Method	#params	CIFAR-10				CIFAR-100			
		ACC \uparrow	ECE \downarrow	NLL \downarrow	Brier \downarrow	ACC \uparrow	ECE \downarrow	NLL \downarrow	Brier \downarrow
Teacher ViT (7 layers)	6.27M	83.84 \pm 0.09	12.51 \pm 0.20	10.91 \pm 0.39	28.03 \pm 0.15	52.94 \pm 0.63	30.73 \pm 0.61	32.71 \pm 0.91	74.72 \pm 1.20
Student ViT (3 layers)	2.75M	82.20 \pm 0.80	10.92 \pm 1.53	7.90 \pm 0.80	28.58 \pm 1.20	54.86 \pm 0.65	30.12 \pm 0.39	31.25 \pm 0.53	72.17 \pm 0.78
	DiT	2.70M	84.77 \pm 0.63	11.93 \pm 0.51	10.26 \pm 0.52	26.55 \pm 1.17	57.56 \pm 0.37	27.37 \pm 0.62	27.10 \pm 0.77
DIRECTOR	2.70M	85.67\pm0.88	9.67\pm0.62	6.94\pm0.52	23.54\pm1.46	57.79\pm0.57	22.31\pm0.49	22.16\pm0.36	62.57\pm0.85

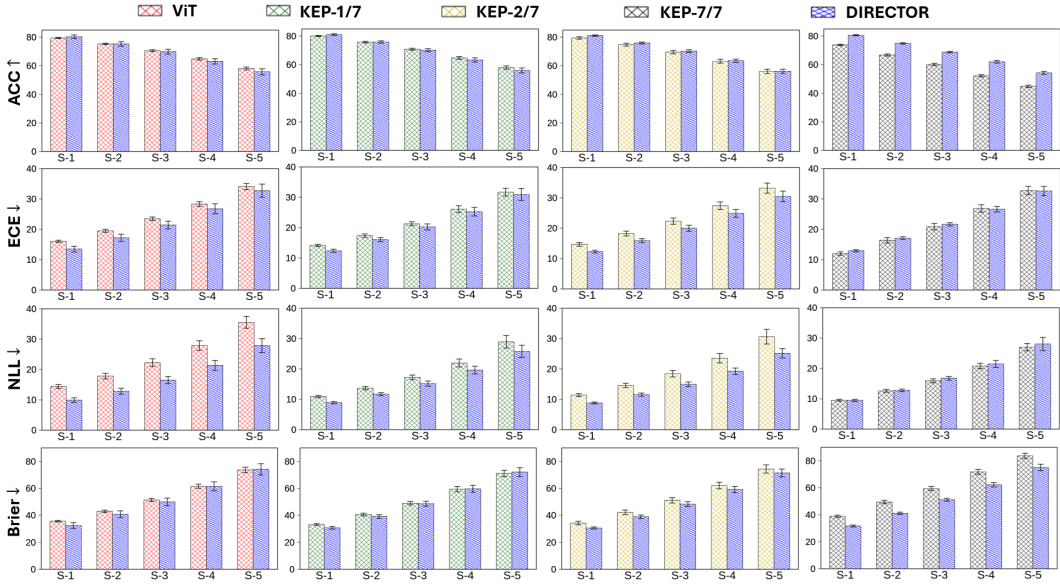


Figure 3: Calibration comparison of pre-trained models with their corresponding diffusion-based reconfigured produced by DIRECTOR on CIFAR-10-C over 5 severity levels of corruption. The notation S- k represents the severity level k . DIRECTOR achieves competitive accuracy and outperforms pre-trained models in most calibration metrics.

Finally, Table 18 compares DIRECTOR against pre-trained models (Transformer and KEP) and other baselines on the CoLA OOD dataset. DIRECTOR achieves the highest MCC score, outperforming all baselines, and shows significant gains in both calibration and failure prediction metrics.

A.6.12 Effect of Varying Loss Weights

We perform extensive ablation studies on the loss weight configurations to investigate their impact on DIRECTOR’s performance on both the CoLA and CIFAR-10 datasets. Specifically, we examine how varying the weights assigned to the mean matching term (λ_{mean}), the Cholesky-like factor alignment (λ_{chol}), and the performance-aware loss (λ_{NLL}) affects both predictive accuracy and uncertainty calibration. When applying diffusion-based reconfiguration with DIRECTOR to KEP-5/5 on CoLA (see Table 19), we observe distinct trends: excessively high λ_{mean} , as in the configuration (0.9, 0.05, 0.05), produces very strong calibration while maintaining decent predictive performance. Conversely, assigning too much weight to λ_{NLL} , as in (0.05, 0.05, 0.9), prioritizes accuracy at the expense of calibration, leading to more confident yet less well-calibrated predictions. Intermediate configurations, such as (0.5, 0.2, 0.3), provide a balanced trade-off, achieving high predictive performance while significantly improving calibration. Based on these insights, we adopt (0.5, 0.2, 0.3) consistently for all diffusion-based reconfigured KEP produced by DIRECTOR, as it offers the most reliable combination of accuracy and calibrated uncertainty.

We also study the effect of varying the weights for the mean matching term (λ_{mean}) and the performance-aware loss (λ_{NLL}) while setting $\lambda_{\text{chol}} = 0$ during diffusion-based reconfiguring ViT

Table 16: Performance comparison for in-distribution classification across four tasks. $\text{KEP-}k/n$ denotes a pre-trained transformer using GP-reparameterized architecture (KEP [15]) for the last k attention blocks and standard MHSA for the remaining blocks. **Bold** indicates the better performance in each pairwise comparison between a pre-trained model (ViT, Transformer, KEP) and diffusion-based reconfigured KEP [15] produced by DIRECTOR . **Blue** marks the best result across all baselines for a dataset, and **brown** denotes the second-best.

Dataset	Method	ACC/MCC \uparrow	AURC \downarrow	AUROC \uparrow	FPR95 \downarrow	ECE \downarrow	NLL \downarrow	Brier \downarrow
CIFAR-10	TS	83.84 \pm 0.09	3.88 \pm 0.10	86.82 \pm 0.37	65.99 \pm 1.94	9.22 \pm 0.36	6.58 \pm 0.16	25.50 \pm 0.13
	MCD	84.06 \pm 0.23	8.65 \pm 0.03	86.51 \pm 0.32	66.15 \pm 0.60	9.47 \pm 0.16	8.36 \pm 0.32	25.45 \pm 0.29
	KFLLA	83.84 \pm 0.10	3.91 \pm 0.11	86.71 \pm 0.45	65.44 \pm 1.58	8.18 \pm 0.80	6.09 \pm 0.40	24.98 \pm 0.59
	SV-DKL	83.23 \pm 0.17	4.39 \pm 0.18	85.94 \pm 0.36	66.96 \pm 1.30	11.64 \pm 0.81	9.85 \pm 1.09	27.97 \pm 0.77
	SGPA	75.59 \pm 3.63	8.41 \pm 2.37	82.65 \pm 1.71	71.78 \pm 2.73	1.92 \pm 0.55	7.11 \pm 0.95	33.98 \pm 4.57
	ViT	83.84 \pm 0.09	4.05 \pm 0.11	86.42 \pm 0.37	67.13 \pm 1.98	12.51 \pm 0.20	10.91 \pm 0.39	28.03 \pm 0.15
	DIRECTOR	85.67 \pm 0.88	3.10 \pm 0.45	87.90 \pm 1.04	61.92 \pm 1.85	9.67 \pm 0.62	6.94 \pm 0.52	23.54 \pm 1.46
	KEP-1/7	84.52 \pm 0.25	3.52 \pm 0.11	87.52 \pm 0.27	65.14 \pm 1.27	10.93 \pm 0.26	8.21 \pm 0.15	25.80 \pm 0.40
	DIRECTOR	86.51 \pm 0.57	2.78 \pm 0.16	88.28 \pm 0.16	61.85 \pm 1.93	8.61 \pm 0.49	6.11 \pm 0.27	21.90 \pm 0.82
	KEP-2/7	84.32 \pm 0.75	3.65 \pm 0.22	87.17 \pm 0.35	65.30 \pm 1.35	11.11 \pm 0.46	8.43 \pm 0.26	26.20 \pm 1.08
	DIRECTOR	86.62 \pm 0.18	2.70 \pm 0.07	88.52 \pm 0.36	60.70 \pm 2.31	8.54 \pm 0.14	5.96 \pm 0.14	21.59 \pm 0.25
	KEP-7/7	82.68 \pm 0.12	4.46 \pm 0.05	85.71 \pm 0.34	66.90 \pm 1.78	6.95 \pm 0.36	5.89 \pm 0.11	25.90 \pm 0.23
DIRECTOR	84.74 \pm 0.40	3.47 \pm 0.18	87.34 \pm 0.33	62.88 \pm 1.20	5.18 \pm 0.33	4.84 \pm 0.11	22.48 \pm 0.53	
CIFAR-100	TS	52.94 \pm 0.63	22.34 \pm 0.61	82.29 \pm 0.48	71.65 \pm 1.98	17.06 \pm 0.42	21.57 \pm 0.52	64.77 \pm 0.95
	MCD	53.49 \pm 0.62	22.24 \pm 0.56	81.60 \pm 0.19	73.02 \pm 0.51	25.93 \pm 0.37	29.24 \pm 0.73	70.02 \pm 0.92
	KFLLA	52.27 \pm 0.86	23.96 \pm 0.78	81.30 \pm 0.48	71.42 \pm 1.92	18.52 \pm 5.40	20.89 \pm 0.57	66.51 \pm 1.66
	SV-DKL	51.03 \pm 0.60	24.38 \pm 0.43	81.32 \pm 0.50	73.99 \pm 1.40	25.46 \pm 0.72	28.93 \pm 0.66	71.90 \pm 0.74
	SGPA	52.77 \pm 0.52	22.84 \pm 0.52	81.65 \pm 0.36	72.02 \pm 1.74	10.33 \pm 2.25	19.10 \pm 0.57	62.08 \pm 1.04
	ViT	52.94 \pm 0.63	22.88 \pm 0.64	81.07 \pm 0.56	75.96 \pm 2.39	30.73 \pm 0.61	32.71 \pm 0.91	74.72 \pm 1.20
	DIRECTOR	57.79 \pm 0.57	18.58 \pm 0.37	82.60 \pm 0.11	71.50 \pm 1.42	22.31 \pm 0.49	22.16 \pm 0.36	62.57 \pm 0.85
	KEP-1/7	55.74 \pm 0.77	20.20 \pm 0.64	82.10 \pm 0.20	73.82 \pm 0.92	27.07 \pm 0.71	27.45 \pm 0.62	68.54 \pm 1.18
	DIRECTOR	58.78 \pm 1.52	17.63 \pm 1.08	82.99 \pm 0.41	71.40 \pm 1.24	21.17 \pm 1.03	21.15 \pm 0.93	60.96 \pm 1.73
	KEP-2/7	55.82 \pm 1.12	20.14 \pm 0.94	82.16 \pm 0.32	73.34 \pm 1.05	27.37 \pm 0.55	27.74 \pm 0.51	68.65 \pm 1.42
	DIRECTOR	59.45 \pm 1.06	17.10 \pm 0.80	83.27 \pm 0.33	69.94 \pm 1.33	21.44 \pm 0.86	20.85 \pm 0.49	60.15 \pm 1.16
	KEP-7/7	57.06 \pm 0.56	19.38 \pm 0.60	82.02 \pm 0.39	72.78 \pm 0.69	21.31 \pm 3.85	22.41 \pm 2.29	63.07 \pm 2.11
DIRECTOR	60.85 \pm 2.98	16.35 \pm 2.34	82.91 \pm 0.67	71.46 \pm 1.43	21.43 \pm 2.09	20.55 \pm 2.42	58.91 \pm 4.63	
IMDB	TS	85.59 \pm 0.50	4.73 \pm 0.32	80.75 \pm 0.55	75.45 \pm 1.10	2.91 \pm 1.51	3.41 \pm 0.13	21.04 \pm 0.74
	MCD	85.96 \pm 0.42	4.40 \pm 0.24	81.40 \pm 0.55	74.79 \pm 0.88	4.18 \pm 2.03	3.47 \pm 0.23	20.72 \pm 0.82
	KFLLA	85.59 \pm 0.50	4.71 \pm 0.30	80.82 \pm 0.48	75.45 \pm 1.11	5.84 \pm 2.21	6.93 \pm 0.00	21.86 \pm 1.19
	SV-DKL	85.69 \pm 0.66	5.58 \pm 0.79	78.54 \pm 2.20	75.32 \pm 0.84	8.52 \pm 1.57	4.49 \pm 0.65	23.10 \pm 1.66
	SGPA	85.39 \pm 0.36	4.96 \pm 0.49	80.04 \pm 1.14	76.44 \pm 0.96	6.04 \pm 1.71	3.96 \pm 0.50	22.19 \pm 1.06
	Transformer	85.59 \pm 0.50	4.73 \pm 0.32	80.75 \pm 0.55	75.45 \pm 1.10	6.96 \pm 2.05	3.95 \pm 0.44	22.28 \pm 1.26
	DIRECTOR	86.07 \pm 0.61	4.57 \pm 0.39	80.84 \pm 0.67	74.24 \pm 0.87	5.40 \pm 1.90	3.60 \pm 0.34	21.08 \pm 1.32
	KEP-1/5	85.76 \pm 0.71	4.54 \pm 0.42	81.02 \pm 0.70	74.87 \pm 0.87	5.51 \pm 2.94	3.79 \pm 0.51	21.62 \pm 1.42
	DIRECTOR	87.13 \pm 0.19	4.07 \pm 0.30	81.55 \pm 0.62	73.35 \pm 0.14	3.16 \pm 2.54	3.24 \pm 0.31	19.31 \pm 0.97
	KEP-2/5	86.52 \pm 0.72	4.18 \pm 0.37	81.54 \pm 0.54	73.82 \pm 1.68	5.72 \pm 1.20	3.58 \pm 0.29	20.51 \pm 1.16
	DIRECTOR	86.95 \pm 0.19	4.05 \pm 0.30	81.64 \pm 0.85	73.46 \pm 1.34	3.46 \pm 1.40	3.23 \pm 0.13	19.42 \pm 0.49
	KEP-5/5	84.57 \pm 0.81	5.48 \pm 0.60	79.32 \pm 1.25	77.03 \pm 1.48	7.83 \pm 3.28	5.17 \pm 2.13	24.23 \pm 2.56
DIRECTOR	85.74 \pm 0.34	4.58 \pm 0.23	80.95 \pm 0.42	75.08 \pm 1.15	2.33 \pm 1.54	3.36 \pm 0.12	20.70 \pm 0.65	
CoLA	TS	29.92 \pm 1.17	20.84 \pm 1.23	64.31 \pm 1.44	89.93 \pm 2.95	23.22 \pm 2.99	11.04 \pm 1.91	51.70 \pm 3.42
	MCD	30.04 \pm 1.02	20.66 \pm 1.11	64.53 \pm 1.00	89.51 \pm 1.35	24.96 \pm 1.79	17.83 \pm 3.61	53.52 \pm 2.59
	KFLLA	29.89 \pm 1.14	20.82 \pm 1.26	64.22 \pm 1.46	89.87 \pm 3.24	24.36 \pm 2.25	12.16 \pm 1.49	52.80 \pm 2.85
	SV-DKL	30.07 \pm 1.41	22.76 \pm 2.28	61.98 \pm 3.09	89.00 \pm 2.55	25.71 \pm 1.60	17.96 \pm 3.26	54.40 \pm 2.13
	SGPA	31.53 \pm 2.05	20.44 \pm 2.60	64.34 \pm 1.95	90.79 \pm 0.87	26.22 \pm 1.51	28.65 \pm 7.23	54.08 \pm 2.44
	Transformer	29.92 \pm 1.17	20.80 \pm 1.21	64.22 \pm 1.46	90.01 \pm 2.84	26.44 \pm 1.90	19.66 \pm 4.18	55.09 \pm 2.68
	DIRECTOR	31.85 \pm 2.46	19.74 \pm 1.62	64.52 \pm 1.71	89.52 \pm 3.61	23.94 \pm 0.49	14.29 \pm 3.01	50.82 \pm 1.19
	KEP-1/5	30.86 \pm 2.03	19.86 \pm 2.04	65.18 \pm 1.83	89.10 \pm 2.60	24.98 \pm 2.08	16.28 \pm 4.35	52.86 \pm 2.88
	DIRECTOR	31.84 \pm 1.88	19.42 \pm 1.83	65.54 \pm 1.78	90.37 \pm 0.89	13.77 \pm 6.58	8.26 \pm 3.75	43.54 \pm 3.65
	KEP-2/5	30.73 \pm 2.29	20.36 \pm 1.40	64.03 \pm 1.21	90.23 \pm 1.86	21.78 \pm 6.62	15.52 \pm 7.74	50.14 \pm 5.92
	DIRECTOR	33.03 \pm 1.36	19.06 \pm 3.05	64.78 \pm 2.31	89.79 \pm 2.65	11.45 \pm 4.78	6.72 \pm 0.98	41.64 \pm 3.58
	KEP-5/5	29.28 \pm 1.21	20.82 \pm 1.98	64.47 \pm 0.90	89.65 \pm 1.04	18.95 \pm 5.66	11.83 \pm 7.96	48.65 \pm 5.84
DIRECTOR	32.05 \pm 1.56	18.69 \pm 1.39	64.71 \pm 1.37	89.53 \pm 1.67	12.88 \pm 5.74	7.68 \pm 1.70	42.20 \pm 2.50	

Table 17: Performance comparison on CIFAR-10-C, with 15 corruptions across five severity levels over five trials.

Method	ACC \uparrow	AURC \downarrow	AUROC \uparrow	FPR95 \downarrow	ECE \downarrow	NLL \downarrow	Brier \downarrow
MCD	69.73 \pm 0.36	14.46 \pm 0.22	79.11 \pm 0.11	76.96 \pm 0.20	19.58 \pm 0.23	18.48 \pm 0.67	48.70 \pm 0.47
KFLLA	69.64 \pm 0.43	14.46 \pm 0.41	79.27 \pm 0.23	76.34 \pm 0.33	17.46 \pm 1.18	12.75 \pm 0.80	47.18 \pm 1.06
SVDKL	68.88 \pm 0.36	15.43 \pm 0.56	78.56 \pm 0.50	77.22 \pm 0.55	22.67 \pm 1.18	21.02 \pm 2.57	52.29 \pm 1.35
SGPA	57.73 \pm 1.25	24.82 \pm 1.23	74.81 \pm 0.65	80.92 \pm 0.54	12.47 \pm 2.11	13.60 \pm 0.48	57.91 \pm 1.39
ViT	69.67 \pm 0.34	14.66 \pm 0.27	78.92 \pm 0.16	77.74 \pm 0.28	24.30 \pm 0.31	23.59 \pm 1.00	53.07 \pm 0.59
DIRECTOR	68.89 \pm 1.44	15.31 \pm 1.30	79.17 \pm 0.86	77.10 \pm 1.00	22.32 \pm 1.09	17.71 \pm 1.02	51.77 \pm 2.39
KEP-1/7	69.87 \pm 0.45	14.30 \pm 0.50	79.49 \pm 0.38	76.95 \pm 0.43	22.12 \pm 0.47	18.54 \pm 0.63	50.65 \pm 0.90
DIRECTOR	69.29 \pm 0.66	15.00 \pm 0.69	79.69 \pm 0.27	76.38 \pm 0.40	20.98 \pm 0.65	16.23 \pm 0.60	50.07 \pm 1.20
KEP-2/7	68.63 \pm 0.75	15.46 \pm 0.66	78.90 \pm 0.37	77.57 \pm 0.42	23.18 \pm 0.63	19.72 \pm 0.76	52.82 \pm 1.30
DIRECTOR	69.41 \pm 0.55	14.95 \pm 0.60	79.73 \pm 0.42	76.29 \pm 0.73	20.71 \pm 0.63	15.94 \pm 0.44	49.71 \pm 1.10
KEP-7/7	59.57 \pm 0.30	23.77 \pm 0.40	75.56 \pm 0.30	80.47 \pm 0.27	21.78 \pm 0.59	17.17 \pm 0.39	60.67 \pm 0.72
DIRECTOR	68.12 \pm 0.26	16.45 \pm 0.28	79.08 \pm 0.22	76.73 \pm 0.29	22.19 \pm 0.19	17.70 \pm 0.17	52.27 \pm 0.35

Table 18: Performance comparison on CoLA OOD over five trials.

Method	MCC \uparrow	AURC \downarrow	AUROC \uparrow	FPR95 \downarrow	ECE \downarrow	NLL \downarrow	Brier \downarrow
MC Dropout	18.54 \pm 4.14	25.85 \pm 1.03	63.31 \pm 2.18	90.17 \pm 2.95	32.02 \pm 2.56	23.84 \pm 5.19	65.50 \pm 4.46
KFLLA	18.43 \pm 3.55	25.89 \pm 0.99	63.31 \pm 1.65	90.50 \pm 3.25	29.94 \pm 2.86	14.64 \pm 1.87	62.72 \pm 4.37
SVDKL	19.32 \pm 3.57	27.58 \pm 2.51	60.65 \pm 1.41	89.97 \pm 2.67	30.97 \pm 3.10	21.23 \pm 3.67	64.07 \pm 4.62
SGPA	19.34 \pm 6.23	27.48 \pm 2.55	61.68 \pm 2.29	90.14 \pm 2.30	31.15 \pm 1.66	35.18 \pm 8.59	63.62 \pm 3.65
Transformer	18.43 \pm 3.55	25.85 \pm 1.00	63.38 \pm 1.69	90.39 \pm 3.27	31.99 \pm 2.70	23.82 \pm 5.16	65.50 \pm 4.32
DIRECTOR	23.06 \pm 4.69	25.61 \pm 2.30	61.32 \pm 3.21	88.23 \pm 3.89	28.72 \pm 1.87	17.18 \pm 3.75	59.91 \pm 2.20
KEP-1/5	19.44 \pm 1.94	25.21 \pm 1.53	63.65 \pm 3.19	87.35 \pm 2.43	30.33 \pm 1.48	19.67 \pm 4.82	61.97 \pm 2.25
DIRECTOR	22.10 \pm 5.49	24.91 \pm 1.80	62.23 \pm 2.98	91.55 \pm 3.19	17.50 \pm 7.52	9.34 \pm 4.50	49.92 \pm 5.80
KEP-2/5	20.38 \pm 5.22	24.39 \pm 2.05	63.60 \pm 1.71	90.75 \pm 2.62	26.04 \pm 7.51	17.94 \pm 9.12	57.77 \pm 8.04
DIRECTOR	20.11 \pm 2.48	23.23 \pm 2.36	63.62 \pm 0.91	89.81 \pm 1.37	15.67 \pm 5.90	7.64 \pm 1.45	48.23 \pm 5.01
KEP-5/5	21.14 \pm 3.48	24.06 \pm 2.27	63.33 \pm 1.36	90.46 \pm 2.20	23.27 \pm 6.61	14.25 \pm 10.66	55.12 \pm 7.78
DIRECTOR	20.20 \pm 5.46	21.97 \pm 1.72	65.12 \pm 1.63	90.17 \pm 3.89	17.49 \pm 5.93	8.61 \pm 1.99	48.55 \pm 3.67

with DIRECTOR on CIFAR-10 (Table 20). When λ_{mean} is excluded (e.g., (0.0, 1.0)), the NLL term dominates, which may slightly improve calibration but leads to reduced predictive performance. In contrast, including both mean matching ($\lambda_{\text{mean}} \neq 0$) and performance-aware loss consistently enhances accuracy and uncertainty calibration. Notably, the configuration (0.8, 0.2) achieves the best overall balance, with the highest accuracy (87.16) and lowest ECE (8.54). Consequently, we adopt (0.8, 0.2) for all diffusion-based reconfigured ViT produced by DIRECTOR.

A.6.13 Training Configuration and Learning Dynamics

Pre-trained transformer-based models. We reproduce the pre-trained ViT and KEP-SVGP models following the experimental settings in [15], as their weights are not publicly available. To ensure that the reproduced models converge properly, we report training loss and validation accuracy over epochs for ViT and KEP-7/7 on CIFAR-10 in Figure 4. The curves indicate stable convergence for both architectures, providing a reliable starting point for subsequent reconfiguration.

DIRECTOR. Building on these pre-trained models, we reconfigure each using a DiT-based unified transition model that takes (X_t, t) as input and outputs the feature representation at diffusion step t . This unified spatiotemporal transition model is implemented using a single-block DiT, which conditions on the diffusion timestep via adaptive LayerNorm-zero (AdaLN-Zero). We adopt the default DiT configuration while adjusting the model dimension d_{model} to match the corresponding pre-trained backbone, ensuring compatibility. For reproducibility, all training hyperparameters for the unified transition model are summarized in Table 21.

A.7 Broader Impact

This work advances the reliability and interpretability of large pre-trained Transformer models by enabling principled uncertainty calibration, a critical requirement for deploying AI in high stakes domains such as healthcare, autonomous systems, and scientific discovery. By introducing a

Table 19: Ablation on loss weighting on CoLA when diffusion-based reconfiguring KEP-5/5 with DIRECTOR. We report mean \pm std across 5 seeds. The configuration $(\lambda_{\text{mean}}, \lambda_{\text{Chol}}, \lambda_{\text{NLL}}) = (0.5, 0.2, 0.3)$ (gray) is chosen as it balances predictive performance (MCC) with uncertainty calibration. This setting is applied consistently for all diffusion-based reconfigured KEP [15] produced by DIRECTOR.

Method	λ_{mean}	λ_{Chol}	λ_{NLL}	MCC \uparrow	ECE \downarrow	NLL \downarrow
Transformers	–	–	–	29.92 \pm 1.17	26.44 \pm 1.90	19.66 \pm 4.18
DIRECTOR	0.9	0.05	0.05	29.98 \pm 3.45	5.96 \pm 4.60	5.86 \pm 0.49
	0.6	0.1	0.3	33.18 \pm 1.53	18.36 \pm 2.29	10.09 \pm 2.38
	0.5	0.3	0.2	32.26 \pm 2.87	15.27 \pm 9.06	9.51 \pm 2.70
	0.5	0.25	0.25	32.96 \pm 1.85	12.27 \pm 8.57	8.23 \pm 2.71
	0.5	0.2	0.3	31.81 \pm 2.30	12.65 \pm 6.04	7.69 \pm 1.70
	0.3	0.2	0.5	31.86 \pm 2.79	18.64 \pm 8.43	13.77 \pm 7.32
	0.3	0.1	0.6	30.21 \pm 2.32	16.50 \pm 8.60	10.74 \pm 5.80
	0.25	0.25	0.5	33.38 \pm 2.08	22.26 \pm 3.72	15.10 \pm 4.85
	0.05	0.05	0.9	30.74 \pm 1.44	15.50 \pm 6.34	9.52 \pm 4.12

Table 20: Ablation on loss weighting on CIFAR-10 (single run) when reconfiguring ViT with DIRECTOR. We report test accuracy (ACC), Expected Calibration Error (ECE), and Negative Log-Likelihood (NLL). The configuration $(\lambda_{\text{mean}}, \lambda_{\text{NLL}}) = (0.8, 0.2)$ (gray) is selected as it achieves the best balance between accuracy and calibration, and is used for all diffusion-based reconfigured ViT produced by DIRECTOR.

Method	λ_{mean}	λ_{NLL}	ACC \uparrow	AURC \downarrow	AUROC \uparrow	FPR95 \downarrow	ECE \downarrow	NLL \downarrow	Brier \downarrow
ViT	–	–	84.22	3.90	86.62	65.34	12.39	10.67	27.52
DIRECTOR	0.0	1.0	84.03	4.01	85.97	67.81	12.12	9.69	27.49
	0.1	0.9	85.24	3.26	87.54	62.87	10.97	8.51	24.99
	0.2	0.8	85.67	3.03	88.16	61.83	10.52	7.75	24.11
	0.3	0.7	86.08	3.06	87.57	59.91	10.24	7.86	23.44
	0.4	0.6	86.05	2.91	88.51	62.22	10.25	7.61	23.45
	0.5	0.5	86.18	2.86	88.21	63.89	9.97	7.41	23.45
	0.6	0.4	86.60	2.83	87.81	64.93	9.50	6.98	22.58
	0.7	0.3	86.66	2.73	88.39	61.02	9.18	6.74	22.05
	0.8	0.2	87.16	2.52	88.92	57.94	8.54	6.06	20.99
	0.9	0.1	85.09	3.54	86.73	64.19	10.15	7.37	24.79

scalable framework for embedding probabilistic reasoning within existing architectures, our approach promotes safer and more accountable AI systems. Additionally, it opens new opportunities for research in uncertainty-aware foundation models and supports the responsible use of AI in socially impactful applications.

A.8 Limitations

While our approach enables principled uncertainty propagation in pre-trained Transformers, it introduces additional computational overhead by absorbing the pre-trained probability path into the propagation model. As the propagation model must be configured with a size compatible with that of the pre-trained model, the computational cost grows proportionally with model scale. Consequently, large-scale or very deep architectures in real-world settings require further investigation to validate the efficacy of the proposed method, which we leave for future work due to computational constraints. In addition, although we demonstrate strong empirical performance across vision and language tasks, further evaluation is needed in domains with sparse supervision or non-stationary data distributions.

Table 21: Hyperparameters for unified transition model training.

Hyperparameters	Settings
d_{model}	384 (CV), 256 (CoLA), 128 (IMDB)
Number of attention heads	12 (CV), 8 (CoLA), 4 (IMDB)
Depth of DiT	1
Epochs	100 (CV), 50 (NLP)
Batch size	128 (CV), 32 (NLP)
Dropout	0.1
Optimizer	Adam
Learning rate	1e-3 (CV), 5e-3 (NLP)
Adam β	(0.9, 0.999)
Weight decay	1e-5
Scheduler	CosineAnnealingLR
Cosine cycle epochs	50
Minimal learning rate	1e-5
Warmup Epochs	5

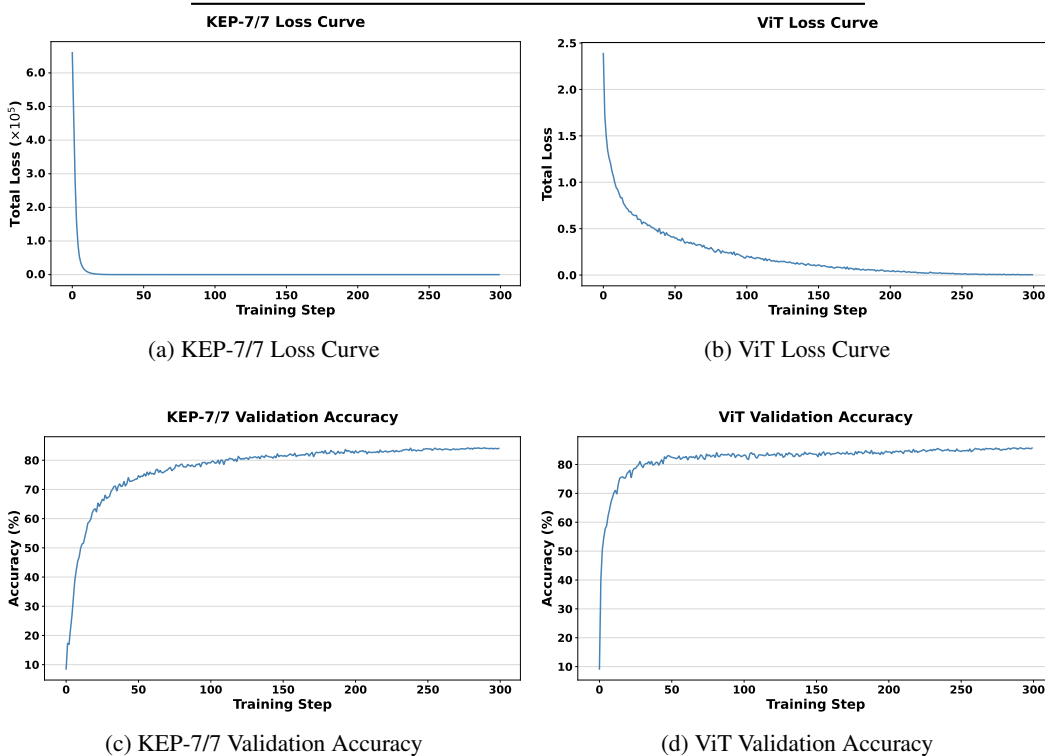


Figure 4: Training curves comparison between KEP-7/7 and ViT models. (a) and (b) show the loss curves, while (c) and (d) show the validation accuracy over training steps.

NeurIPS Paper Checklist

1. Claims

Question: Do the main claims made in the abstract and introduction accurately reflect the paper’s contributions and scope?

Answer: [Yes]

Justification: The contributions are summarised in the abstract and Section 1, and substantiated by the experiments in Section 3 and Appendix A.6.

Guidelines:

- The answer [N/A] means that the abstract and introduction do not include the claims made in the paper.

- The abstract and/or introduction should clearly state the claims made, including the contributions made in the paper and important assumptions and limitations. A [No] or [N/A] answer to this question will not be perceived well by the reviewers.
- The claims made should match theoretical and experimental results, and reflect how much the results can be expected to generalize to other settings.
- It is fine to include aspirational goals as motivation as long as it is clear that these goals are not attained by the paper.

2. Limitations

Question: Does the paper discuss the limitations of the work performed by the authors?

Answer: [Yes]

Justification: We discuss this in Appendix A.8, including the scale of the evaluated backbones and the iterative-sampling cost of diffusion-based propagation.

Guidelines:

- The answer [N/A] means that the paper has no limitation while the answer [No] means that the paper has limitations, but those are not discussed in the paper.
- The authors are encouraged to create a separate “Limitations” section in their paper.
- The paper should point out any strong assumptions and how robust the results are to violations of these assumptions (e.g., independence assumptions, noiseless settings, model well-specification, asymptotic approximations only holding locally). The authors should reflect on how these assumptions might be violated in practice and what the implications would be.
- The authors should reflect on the scope of the claims made, e.g., if the approach was only tested on a few datasets or with a few runs. In general, empirical results often depend on implicit assumptions, which should be articulated.
- The authors should reflect on the factors that influence the performance of the approach. For example, a facial recognition algorithm may perform poorly when image resolution is low or images are taken in low lighting. Or a speech-to-text system might not be used reliably to provide closed captions for online lectures because it fails to handle technical jargon.
- The authors should discuss the computational efficiency of the proposed algorithms and how they scale with dataset size.
- If applicable, the authors should discuss possible limitations of their approach to address problems of privacy and fairness.
- While the authors might fear that complete honesty about limitations might be used by reviewers as grounds for rejection, a worse outcome might be that reviewers discover limitations that aren’t acknowledged in the paper. The authors should use their best judgment and recognize that individual actions in favor of transparency play an important role in developing norms that preserve the integrity of the community. Reviewers will be specifically instructed to not penalize honesty concerning limitations.

3. Theory assumptions and proofs

Question: For each theoretical result, does the paper provide the full set of assumptions and a complete (and correct) proof?

Answer: [N/A]

Justification: The paper does not state formal theorems; the variational training objective is derived in Appendix A.5, with the underlying GP and Cholesky-like covariance assumptions stated in Sections 2.1–2.2 and Appendix A.6.5.

Guidelines:

- The answer [N/A] means that the paper does not include theoretical results.
- All the theorems, formulas, and proofs in the paper should be numbered and cross-referenced.
- All assumptions should be clearly stated or referenced in the statement of any theorems.
- The proofs can either appear in the main paper or the supplemental material, but if they appear in the supplemental material, the authors are encouraged to provide a short proof sketch to provide intuition.

- Inversely, any informal proof provided in the core of the paper should be complemented by formal proofs provided in appendix or supplemental material.
- Theorems and Lemmas that the proof relies upon should be properly referenced.

4. Experimental result reproducibility

Question: Does the paper fully disclose all the information needed to reproduce the main experimental results of the paper to the extent that it affects the main claims and/or conclusions of the paper (regardless of whether the code and data are provided or not)?

Answer: [Yes]

Justification: All information needed to reproduce our experiments is provided in Section 3 and Appendix A.6; Algorithm 1 gives the exact training iteration of DIRECTOR.

Guidelines:

- The answer [N/A] means that the paper does not include experiments.
- If the paper includes experiments, a [No] answer to this question will not be perceived well by the reviewers: Making the paper reproducible is important, regardless of whether the code and data are provided or not.
- If the contribution is a dataset and/or model, the authors should describe the steps taken to make their results reproducible or verifiable.
- Depending on the contribution, reproducibility can be accomplished in various ways. For example, if the contribution is a novel architecture, describing the architecture fully might suffice, or if the contribution is a specific model and empirical evaluation, it may be necessary to either make it possible for others to replicate the model with the same dataset, or provide access to the model. In general, releasing code and data is often one good way to accomplish this, but reproducibility can also be provided via detailed instructions for how to replicate the results, access to a hosted model (e.g., in the case of a large language model), releasing of a model checkpoint, or other means that are appropriate to the research performed.
- While NeurIPS does not require releasing code, the conference does require all submissions to provide some reasonable avenue for reproducibility, which may depend on the nature of the contribution. For example
 - (a) If the contribution is primarily a new algorithm, the paper should make it clear how to reproduce that algorithm.
 - (b) If the contribution is primarily a new model architecture, the paper should describe the architecture clearly and fully.
 - (c) If the contribution is a new model (e.g., a large language model), then there should either be a way to access this model for reproducing the results or a way to reproduce the model (e.g., with an open-source dataset or instructions for how to construct the dataset).
 - (d) We recognize that reproducibility may be tricky in some cases, in which case authors are welcome to describe the particular way they provide for reproducibility. In the case of closed-source models, it may be that access to the model is limited in some way (e.g., to registered users), but it should be possible for other researchers to have some path to reproducing or verifying the results.

5. Open access to data and code

Question: Does the paper provide open access to the data and code, with sufficient instructions to faithfully reproduce the main experimental results, as described in supplemental material?

Answer: [Yes]

Justification: All datasets used and pre-trained baselines are publicly available; our experimental code is submitted as supplementary material with this manuscript.

Guidelines:

- The answer [N/A] means that paper does not include experiments requiring code.
- Please see the NeurIPS code and data submission guidelines (<https://neurips.cc/public/guides/CodeSubmissionPolicy>) for more details.

- While we encourage the release of code and data, we understand that this might not be possible, so [No] is an acceptable answer. Papers cannot be rejected simply for not including code, unless this is central to the contribution (e.g., for a new open-source benchmark).
- The instructions should contain the exact command and environment needed to run to reproduce the results. See the NeurIPS code and data submission guidelines (<https://neurips.cc/public/guides/CodeSubmissionPolicy>) for more details.
- The authors should provide instructions on data access and preparation, including how to access the raw data, preprocessed data, intermediate data, and generated data, etc.
- The authors should provide scripts to reproduce all experimental results for the new proposed method and baselines. If only a subset of experiments are reproducible, they should state which ones are omitted from the script and why.
- At submission time, to preserve anonymity, the authors should release anonymized versions (if applicable).
- Providing as much information as possible in supplemental material (appended to the paper) is recommended, but including URLs to data and code is permitted.

6. Experimental setting/details

Question: Does the paper specify all the training and test details (e.g., data splits, hyperparameters, how they were chosen, type of optimizer) necessary to understand the results?

Answer: [Yes]

Justification: Such details can be found in Section 3 and Appendix A.6.13 (Table 21); the loss-weight selection procedure is described in Appendix A.6.12.

Guidelines:

- The answer [N/A] means that the paper does not include experiments.
- The experimental setting should be presented in the core of the paper to a level of detail that is necessary to appreciate the results and make sense of them.
- The full details can be provided either with the code, in appendix, or as supplemental material.

7. Experiment statistical significance

Question: Does the paper report error bars suitably and correctly defined or other appropriate information about the statistical significance of the experiments?

Answer: [Yes]

Justification: All metrics in Tables 1 and 2 are reported as mean \pm standard error over five seeds, and Appendix A.6.8 reports paired *t*-tests for the main comparisons.

Guidelines:

- The answer [N/A] means that the paper does not include experiments.
- The authors should answer [Yes] if the results are accompanied by error bars, confidence intervals, or statistical significance tests, at least for the experiments that support the main claims of the paper.
- The factors of variability that the error bars are capturing should be clearly stated (for example, train/test split, initialization, random drawing of some parameter, or overall run with given experimental conditions).
- The method for calculating the error bars should be explained (closed form formula, call to a library function, bootstrap, etc.)
- The assumptions made should be given (e.g., Normally distributed errors).
- It should be clear whether the error bar is the standard deviation or the standard error of the mean.
- It is OK to report 1-sigma error bars, but one should state it. The authors should preferably report a 2-sigma error bar than state that they have a 96% CI, if the hypothesis of Normality of errors is not verified.
- For asymmetric distributions, the authors should be careful not to show in tables or figures symmetric error bars that would yield results that are out of range (e.g., negative error rates).

- If error bars are reported in tables or plots, the authors should explain in the text how they were calculated and reference the corresponding figures or tables in the text.

8. Experiments compute resources

Question: For each experiment, does the paper provide sufficient information on the computer resources (type of compute workers, memory, time of execution) needed to reproduce the experiments?

Answer: [Yes]

Justification: Section 3 reports the computing resource; Appendix A.6.6 reports per-method inference time and memory, and Table 11 reports stage-1 and stage-2 wall-clock training times on CIFAR-10.

Guidelines:

- The answer [N/A] means that the paper does not include experiments.
- The paper should indicate the type of compute workers CPU or GPU, internal cluster, or cloud provider, including relevant memory and storage.
- The paper should provide the amount of compute required for each of the individual experimental runs as well as estimate the total compute.
- The paper should disclose whether the full research project required more compute than the experiments reported in the paper (e.g., preliminary or failed experiments that didn't make it into the paper).

9. Code of ethics

Question: Does the research conducted in the paper conform, in every respect, with the NeurIPS Code of Ethics <https://neurips.cc/public/EthicsGuidelines?>

Answer: [Yes]

Justification: We have read the NeurIPS Code of Ethics and do not find our work in violation of any aspects.

Guidelines:

- The answer [N/A] means that the authors have not reviewed the NeurIPS Code of Ethics.
- If the authors answer [No], they should explain the special circumstances that require a deviation from the Code of Ethics.
- The authors should make sure to preserve anonymity (e.g., if there is a special consideration due to laws or regulations in their jurisdiction).

10. Broader impacts

Question: Does the paper discuss both potential positive societal impacts and negative societal impacts of the work performed?

Answer: [Yes]

Justification: We discuss broader impacts in Appendix A.7; improved uncertainty calibration benefits the trustworthy deployment of pre-trained transformers in risk-sensitive domains, while we do not introduce content-generating models that pose specific misuse risks.

Guidelines:

- The answer [N/A] means that there is no societal impact of the work performed.
- If the authors answer [N/A] or [No], they should explain why their work has no societal impact or why the paper does not address societal impact.
- Examples of negative societal impacts include potential malicious or unintended uses (e.g., disinformation, generating fake profiles, surveillance), fairness considerations (e.g., deployment of technologies that could make decisions that unfairly impact specific groups), privacy considerations, and security considerations.
- The conference expects that many papers will be foundational research and not tied to particular applications, let alone deployments. However, if there is a direct path to any negative applications, the authors should point it out. For example, it is legitimate to point out that an improvement in the quality of generative models could be used to

generate Deepfakes for disinformation. On the other hand, it is not needed to point out that a generic algorithm for optimizing neural networks could enable people to train models that generate Deepfakes faster.

- The authors should consider possible harms that could arise when the technology is being used as intended and functioning correctly, harms that could arise when the technology is being used as intended but gives incorrect results, and harms following from (intentional or unintentional) misuse of the technology.
- If there are negative societal impacts, the authors could also discuss possible mitigation strategies (e.g., gated release of models, providing defenses in addition to attacks, mechanisms for monitoring misuse, mechanisms to monitor how a system learns from feedback over time, improving the efficiency and accessibility of ML).

11. Safeguards

Question: Does the paper describe safeguards that have been put in place for responsible release of data or models that have a high risk for misuse (e.g., pre-trained language models, image generators, or scraped datasets)?

Answer: [N/A]

Justification: Our work does not release any new datasets or pre-trained generative models with a high risk of misuse; the proposed method is a calibration mechanism applied on top of already-public backbones.

Guidelines:

- The answer [N/A] means that the paper poses no such risks.
- Released models that have a high risk for misuse or dual-use should be released with necessary safeguards to allow for controlled use of the model, for example by requiring that users adhere to usage guidelines or restrictions to access the model or implementing safety filters.
- Datasets that have been scraped from the Internet could pose safety risks. The authors should describe how they avoided releasing unsafe images.
- We recognize that providing effective safeguards is challenging, and many papers do not require this, but we encourage authors to take this into account and make a best faith effort.

12. Licenses for existing assets

Question: Are the creators or original owners of assets (e.g., code, data, models), used in the paper, properly credited and are the license and terms of use explicitly mentioned and properly respected?

Answer: [Yes]

Justification: We cite the source of all datasets and pre-trained models used in our experiments (CIFAR-10/100, IMDB, CoLA, the HuggingFace ViT-B-16 and Qwen-2.5 checkpoints) and use them under their original licences.

Guidelines:

- The answer [N/A] means that the paper does not use existing assets.
- The authors should cite the original paper that produced the code package or dataset.
- The authors should state which version of the asset is used and, if possible, include a URL.
- The name of the license (e.g., CC-BY 4.0) should be included for each asset.
- For scraped data from a particular source (e.g., website), the copyright and terms of service of that source should be provided.
- If assets are released, the license, copyright information, and terms of use in the package should be provided. For popular datasets, paperswithcode.com/datasets has curated licenses for some datasets. Their licensing guide can help determine the license of a dataset.
- For existing datasets that are re-packaged, both the original license and the license of the derived asset (if it has changed) should be provided.

- If this information is not available online, the authors are encouraged to reach out to the asset’s creators.

13. **New assets**

Question: Are new assets introduced in the paper well documented and is the documentation provided alongside the assets?

Answer: [N/A]

Justification: Our work does not release any new datasets or pre-trained models; only training and evaluation code is released as supplementary material.

Guidelines:

- The answer [N/A] means that the paper does not release new assets.
- Researchers should communicate the details of the dataset/code/model as part of their submissions via structured templates. This includes details about training, license, limitations, etc.
- The paper should discuss whether and how consent was obtained from people whose asset is used.
- At submission time, remember to anonymize your assets (if applicable). You can either create an anonymized URL or include an anonymized zip file.

14. **Crowdsourcing and research with human subjects**

Question: For crowdsourcing experiments and research with human subjects, does the paper include the full text of instructions given to participants and screenshots, if applicable, as well as details about compensation (if any)?

Answer: [N/A]

Justification: Our work does not involve crowdsourcing nor research with human subjects.

Guidelines:

- The answer [N/A] means that the paper does not involve crowdsourcing nor research with human subjects.
- Including this information in the supplemental material is fine, but if the main contribution of the paper involves human subjects, then as much detail as possible should be included in the main paper.
- According to the NeurIPS Code of Ethics, workers involved in data collection, curation, or other labor should be paid at least the minimum wage in the country of the data collector.

15. **Institutional review board (IRB) approvals or equivalent for research with human subjects**

Question: Does the paper describe potential risks incurred by study participants, whether such risks were disclosed to the subjects, and whether Institutional Review Board (IRB) approvals (or an equivalent approval/review based on the requirements of your country or institution) were obtained?

Answer: [N/A]

Justification: Our work does not involve crowdsourcing nor research with human subjects.

Guidelines:

- The answer [N/A] means that the paper does not involve crowdsourcing nor research with human subjects.
- Depending on the country in which research is conducted, IRB approval (or equivalent) may be required for any human subjects research. If you obtained IRB approval, you should clearly state this in the paper.
- We recognize that the procedures for this may vary significantly between institutions and locations, and we expect authors to adhere to the NeurIPS Code of Ethics and the guidelines for their institution.
- For initial submissions, do not include any information that would break anonymity (if applicable), such as the institution conducting the review.

16. Declaration of LLM usage

Question: Does the paper describe the usage of LLMs if it is an important, original, or non-standard component of the core methods in this research? Note that if the LLM is used only for writing, editing, or formatting purposes and does *not* impact the core methodology, scientific rigor, or originality of the research, declaration is not required.

Answer: [N/A]

Justification: This research employs LLMs exclusively for editing purposes, with no impact on the core methodology. The Qwen-2.5 model in Appendix A.6 is used as a publicly available pre-trained backbone on which we apply our reconfiguration method, not as a methodological component.

Guidelines:

- The answer [N/A] means that the core method development in this research does not involve LLMs as any important, original, or non-standard components.
- Please refer to our LLM policy in the NeurIPS handbook for what should or should not be described.